










## Climate indices of environmental change in the High Arctic: Study from Hornsund, SW Spitsbergen, 1979–2019

Krzysztof MIGAŁA<sup>1</sup> , Elżbieta ŁEPKOWSKA<sup>2\*</sup> , Marzena OSUCH<sup>3</sup> ,  
Łukasz STACHNIK<sup>1</sup> , Tomasz WAWRZYŃIAK<sup>3</sup> ,  
Dariusz IGNATIUK<sup>2</sup>  and Piotr OWCZAREK<sup>1</sup> 

<sup>1</sup> *Institute of Geography and Regional Development, University of Wrocław,  
Plac Uniwersytecki 1, 50-137 Wrocław, Poland*

<sup>2</sup> *Institute of Earth Sciences, Faculty of Natural Sciences, University of Silesia in Katowice,  
ul. Będzińska 60, 41-200 Sosnowiec, Poland*

<sup>3</sup> *Institute of Geophysics, Polish Academy of Sciences,  
ul. Księcia Janusza 6, 01-452 Warszawa, Poland*

\* *corresponding author <elzbieta.majchrowska@us.edu.pl>*

**Abstract:** An analysis of a suite of climatological indices was undertaken on the basis of long-term (1979–2019) climatological data from the Polish Polar Station in Hornsund, SW Spitsbergen. It was followed by an attempt to assess the scale of their impact on the local environment. The temperature and precipitation indices were based on percentiles of the variables calculated for a population of daily values from the climate normals for 1981–2010. A greater share of both cyclonic and anticyclonic circulations from the S and SW sectors, forcing the advection of warm air masses from the south, was decisive for the trends of change in comparison with the long-term mean. Both extreme precipitation and drought events depend on the 500 hPa geopotential height and precipitable water anomalies, determined by the baric field over the North Atlantic. Climate changes impact on the dynamics of local geoecosystems by causing faster glacier ablation and retreat, permafrost degradation, intensification of the hydrological cycle in glaciated and unglaciated catchments, and changes in the condition and growth of tundra vegetation.

**Keywords:** Arctic, Svalbard, climate change, climate variables, polar region.



## Introduction

Arctic amplification is causing unprecedented rises in air temperatures and higher levels of liquid precipitation in polar regions, especially in the Arctic (Pithan and Mauritsen 2014; IPCC 2019). These changes are likely to continue, increasing both air temperatures and precipitation (Łupikasza *et al.* 2019; IPCC 2021; Liu *et al.* 2021), facilitating rapid glacier recession and thinning (van Pelt *et al.* 2019; Noël *et al.* 2020), permafrost degradation and fragmentation (Schaefer *et al.* 2014; Biskaborn *et al.* 2019; Strand *et al.* 2021), and increasing the ecological risk to the entire ecosystem (Hinzman *et al.* 2013; Anderson *et al.* 2017; Owczarek *et al.* 2021).

The climate change in the High Arctic, as exemplified by the Svalbard archipelago, is much stronger than elsewhere in northern polar latitudes. The air temperature rise in Svalbard is twice as great as the average increase in the Arctic (Nordli *et al.* 2020). This has led to the rapid melting and thinning of glaciers, especially as the average altitude of Svalbard is lower than other regions in the Arctic (Noël *et al.* 2020).

Several meteorological stations in Svalbard provide long-term meteorological data, like air temperature, precipitation and sunshine duration, which enable the climate change trends to be compared with the longest composite series (since 1898) from Svalbard Airport in Longyearbyen (Serreze *et al.* 2014; Isaksen *et al.* 2016; Nordli *et al.* 2020). One of them is at the Polish Polar Station in Hornsund (PPS), in the southernmost fjord in Svalbard, which boasts an over 40-year long climatological dataset. Strong positive trends of air temperature and autumn rainfall have been observed at the PPS, making it a unique site for studying climate change (Wawrzyniak and Osuch 2020). In addition, the positive trend in autumn precipitation is one of the highest in Svalbard (Førland *et al.* 2020). Nonetheless, the meteorological data from the PPS have rarely been analyzed in recent studies (*e.g.*, Serreze *et al.* 2015; Nordli *et al.* 2020; Przybylak and Wszyński 2020; Łupikasza *et al.* 2021).

The environmental conditions of Hornsund are representative of southern Spitsbergen fjords. Hornsund is influenced by Atlantic Waters, but because of its southerly position, it is also affected by less saline, coastal Arctic waters from the Barents Sea (Skagseth *et al.* 2008). These conditions mediate climate change and biodiversity in this area and affect geomorphological and glaciological processes (Weydmann and Kwasniewski 2008; Błaszczuk *et al.* 2013; Muckenhuber *et al.* 2016; Smoła *et al.* 2017; Strzelecki *et al.* 2017; Węśławski *et al.* 2017). Hornsund has been selected as one of the *All Taxon Biodiversity Inventory* (ATBI) sites and, together with Kongsfjorden, situated on the north-west coast of West Spitsbergen, has been designated an European Marine Biodiversity Research Site (Warwick *et al.* 2003). Since 1957, interdisciplinary research has been conducted in Hornsund, often within the framework of international projects

and campaigns (3<sup>rd</sup> International Geophysical Year, 4<sup>th</sup> International Polar Year) with extended in situ measurements (Lewandowski *et al.* 2020).

The present analysis covers daily, monthly and annual air temperatures, positive and negative degree days (PDD, NDD), the sum of precipitation, air humidity, atmospheric pressure, wind speed and direction, sunshine duration, cloudiness and visibility. The data from Hornsund confirm that the greatest warming in the High Arctic is taking place in its Atlantic region, as reflected in the dynamics of local geo-ecosystems (Christiansen *et al.* 2013; Przybylak and Wyszynski 2020; Walsh *et al.* 2020). The mean annual air temperature in Hornsund has increased dramatically, at a rate +1.14°C per decade over the last forty years (1979–2019). During this period, the climate in this area has been warming more than six times faster than the global average rate, which is +0.17°C per decade (NOAA 2020). In addition, there has been a clear positive trend in annual precipitation, *i.e.*, 61.6 mm per decade, as well as conspicuous monthly precipitation increases in September (19.67 mm per decade) and October (13.53 mm per decade). Temperature changes have led not only to the positive trend in precipitation, particularly marked since the 1990s, but also to a greater frequency and intensity of extreme rainfall events (Marsz and Styszyńska 2013). These episodes occur in summer and autumn, generating rainfall that can exceed 50 mm in 24 hrs. The increase in cloudiness during this period (0.12 octas per decade) has resulted in a downward trend in sunshine duration (−8.39 hrs/decade), with a particularly noticeable deterioration in solar radiation in May, the sunniest month (−10.07 hrs/decade). These evident trends in primary climatic variables, reflected in a number of hydro- and bioclimatic indices, have a range of environmental consequences.

On the basis of published, long-term climatological data from the PPS, this paper aims to analyze a suite of climatological indices associated with pluviothermic conditions affecting the supply of energy and moisture to land. In particular, it focuses on evaluating long-term changes in climatological indices directly related to polar environmental changes, such as intense glacier ablation, tundra browning, ground warming, permafrost thaw, rain-on-snow and snow/ice melting. These environmental changes have been widely addressed in current studies from polar regions (Hock 2003; Christiansen *et al.* 2013; Weijers *et al.* 2013; Hjort *et al.* 2014; Panchen and Gorelick 2017; Kellerer-Pirklbauer 2018). This work is complementary to other regional studies using climatological indices (Diaconescu *et al.* 2018; Avila-Diaz *et al.* 2021) recommended by The Expert Team on Climate Change Detection and Indices, but we have included a more comprehensive set of such indices based on total daily precipitation, air temperature, combined air temperature/precipitation and drought indices. In this study, we intend to show and discuss how the climatic variables, expressed in numerous indices, explain the state and the dynamics of local geoeosystems and explain how their values depend on synoptic conditions over the North Atlantic.

## Meteorological data from Hornsund

Hornsund is the southernmost fjord on Spitsbergen, and the PPS, where the data were collected, is situated on its northern shore (Fig. 1). The area is representative of the High Arctic with extremely weak diurnal and strong seasonal patterns (Przybylak 2002, 2016). The meteorological station has conducted continuous meteorological observations and measurements since 1978 (World Meteorological Organization registration number 01003). The weather station is equipped and operates in accordance with WMO measurement regulations and standards.

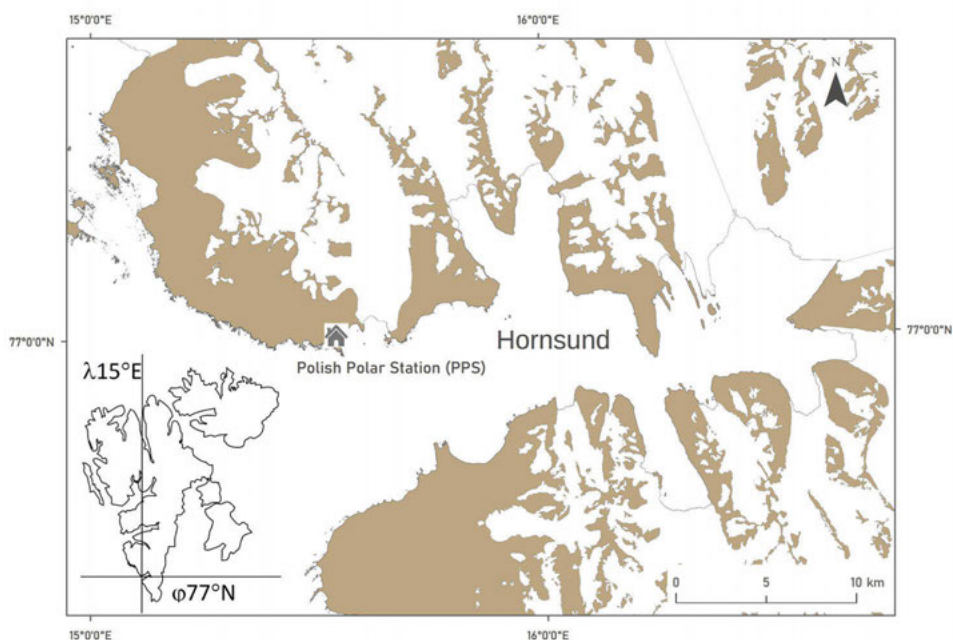


Fig. 1. Location of the study area. Maps reproduced by courtesy of the Norwegian Polar Institute (2014).

During the last 40 years, the mean annual air temperature in the Hornsund area has varied from  $-7.2^{\circ}\text{C}$  (1988) to  $+0.3^{\circ}\text{C}$  (2016) (avg.  $-3.6^{\circ}\text{C}$ ). The average coldest month is March with a mean temperature of  $-10.2^{\circ}\text{C}$ , and the average warmest month is July with a mean temperature of  $+4.6^{\circ}\text{C}$  (Wawrzyniak and Osuch 2020). The average total precipitation is 462.7 mm, the driest month being March with 21.5 mm and the wettest September with 74.9 mm of precipitation. Annual totals have ranged from 230.2 mm (1987) to 805.8 mm in 2016 (Figs. 2 and 3).

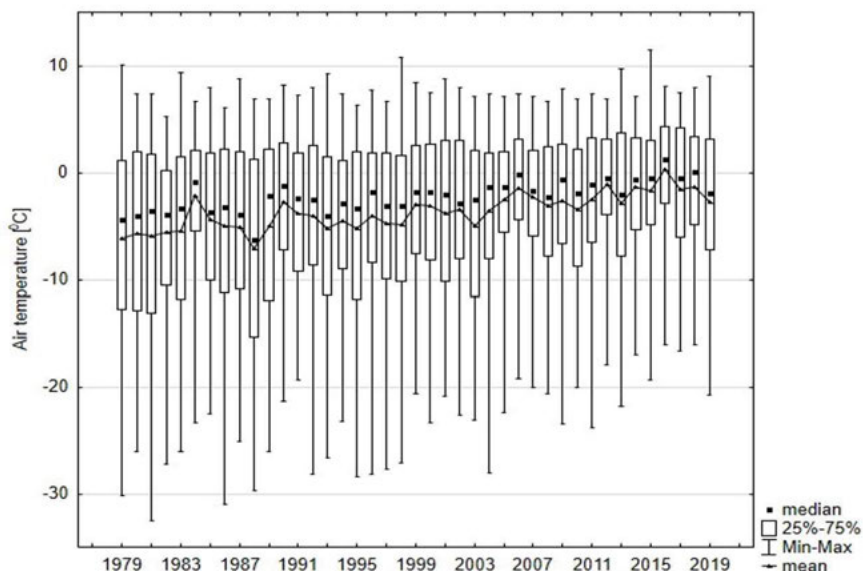


Fig. 2. Variability of the daily air temperature time series between 1979 and 2019 at Hornsund. The boxplots show data for each calendar year.

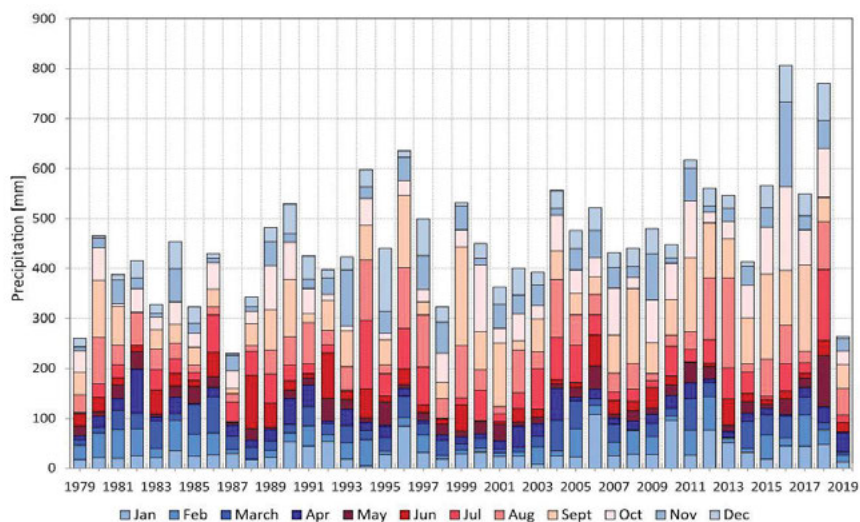


Fig. 3. Annual and monthly precipitation between 1979–2019 at Hornsund.

## Methods

In modest polar ecosystems with a poor heat supply, simple indices based on daily temperatures and precipitation explain the role of heat supply and loss, their amount and duration, the thawing/freezing of water and soil, ice/snow melt, and

the proportions, frequency and intensity of liquid and solid precipitation. For this reason, attention is focused on certain climate indices.

A long-term series of daily air temperature and precipitation from the PPS (Wawrzyniak and Osuch 2019) were used to analyze a suite of climatological variables that play a major role in cold regions and polar ecosystems. The problem of data uncertainty due to changes in the measurement technique and instruments was explained by Wawrzyniak and Osuch (2020), who described the devices and verified the data using a series of statistical tests.

The indices were selected on the basis of recommendations by the European Climate Assessment & Dataset (ECA&D 2013) and by the WMO with respect to drought indices (WMO&GWP 2016). Some of the temperature and precipitation indices were calculated from percentiles of these variables for a population of daily values from 1981–2010 (Table 1). The number of melting days (NMD days with  $T_{\max} \geq 0^{\circ}\text{C}$ ) was also taken into consideration. It can be used as a simple index of snow cover formation (or destruction), as well as the winter component of the glacier mass balance and the initial conditions for the development of an active permafrost layer or vegetation.

The set of indices based on air temperature includes:

NDD – negative degree days, defined as the annual (calendar year) sum of  $T_{\text{avg}} < 0^{\circ}\text{C}$

FDD freezing degree days – the sum of  $T_{\text{avg}} < 0^{\circ}\text{C}$  calculated for the hydrological year (1 September to 31 August)

PDD (TDD) – positive degree days (thawing degree days), defined as the annual sum of  $T_{\text{avg}} > 0^{\circ}\text{C}$  calculated for the calendar year

WSL<sub>0</sub> – warm season length (number of days with  $T_{\text{avg}} > 0^{\circ}\text{C}$ ) \*

GSL<sub>5</sub> – growing season length (number of days with  $T_{\text{avg}} > +5^{\circ}\text{C}$ ) \*

sumT<sub>5</sub> – sum of  $T_{\text{avg}} > +5^{\circ}\text{C}$

GDD<sub>5</sub> – growing degree-days (cumulative daily mean temperature above  $T_{\text{avg}} + 5^{\circ}\text{C}$ );  $\text{GDD}_5 = \Sigma (T_{\text{avg}} - 5^{\circ}\text{C})$

HDD<sub>15.5</sub> – heating degree-days (energy needed to heat a building) – sum of temperatures above the 15.5°C threshold;  $\text{HDD}_{15.5} = \Sigma (15.5^{\circ}\text{C} - T_{\text{avg}})$

FD – frost days – number of days with daily minimum temperature below 0°C and mean temperature above 0°C

ID – icing days – number of days with daily maximum temperature below 0°C

NMD<sub>XI</sub>... NMD<sub>XII</sub> – number of melting days in a given month (days with  $T_{\max} \geq 0^{\circ}\text{C}$ )

NMD<sub>XI-I</sub> – number of melting days during winter months XI–I (days with  $T_{\max} \geq 0^{\circ}\text{C}$ )

NMD<sub>XII-II</sub> – number of melting days during winter months XII–II (days with  $T_{\max} \geq 0^{\circ}\text{C}$ )

NMD<sub>I-IV</sub> – number of melting days during winter months I–IV (days with  $T_{\max} \geq 0^{\circ}\text{C}$ )

$T_{avg}^{90p}$  – number of warm days (days with  $T_{avg} > 90^{th}$  percentile of daily mean temperature)

$T_{avg}^{10p}$  – number of cold days (days with  $T_{avg} < 10^{th}$  percentile of daily mean temperature).

\* Taking into account the number of days between the first occurrence of at least 6 consecutive days above the threshold value and the first occurrence of at least 6 consecutive days below the threshold value.

Indices based on temperature and precipitation:

CD cold/dry days – days with  $T_{avg} < 25^{th}$  percentile of daily mean temperature and  $R < 25^{th}$  percentile of total daily precipitation (cold/dry days)

CW cold/wet days – days with  $T_{avg} < 25^{th}$  percentile of daily mean temperature and  $R > 75^{th}$  percentile of total daily precipitation (cold/wet days)

WD warm/dry days – days with  $T_{avg} > 75^{th}$  percentile of daily mean temperature and  $R < 25^{th}$  percentile of total daily precipitation (warm/dry days)

WW warm/wet days – days with  $T_{avg} > 75^{th}$  percentile of daily mean temperature and  $R > 75^{th}$  percentile of total daily precipitation (warm/wet days)

Indices based on total daily precipitation (R) describing pluvial conditions:

RR1 – wet days ( $R \geq 1$  mm) (days)

SDII – simple daily intensity index (mm/wet day) – computed by dividing the total precipitation on wet days by the number of wet days in the period.

R10 – days with heavy precipitation (precipitation  $\geq 10$  mm) (days)

R20 – days with very heavy precipitation (precipitation  $\geq 20$  mm) (days)

R75p – days with  $RR > 75^{th}$  percentile of daily totals (number of moderately wet days)

R95p – days with  $RR > 95^{th}$  percentile of daily totals (number of very wet days)

R99p – days with  $RR > 99^{th}$  percentile of daily totals (number of extremely wet days)

Drought indices (calculated for months, quarters, half year and year):

SPI Standardized Precipitation Index – based on precipitation as a standard deviation from the long-term average (+ indicates wet; – indices dry).

SPEI Standardized Precipitation Evapotranspiration Index – based on monthly precipitation and temperature, combines SPI with information about potential evapotranspiration.

Reanalysis products provided by the NOAA/ESRL Physical Sciences Laboratory, Boulder, Colorado (<http://psl.noaa.gov>) were used to document the synoptic conditions over the North Atlantic Ocean governing extreme pluviothermic episodes in Spitsbergen. The datasets include daily composites (averages) of the mean or anomalies (mean minus total mean) of variables from the NCEP/NCAR Reanalysis and other datasets. The plots were generated for selected extreme weather situations. The following variables were used: sea level pressure, air temperature anomaly, anomaly of 500 hPa in geopotential height, omega index for 500 hPa explaining the vertical motion of air masses, and the precipitable water anomaly at 1000–500 hPa.

## Results

The estimated values of the indices describing the climatic conditions in the vicinity of the PPS are presented in Table 2 and the Supplementary tables. Most indices show statistically significant upward trends (NDD, FDD, PDD, WSL<sub>0</sub>, WSL<sub>2.5</sub>, sumT<sub>2.5</sub>, GDD<sub>2.5</sub>, GDD<sub>5</sub>, FD, NMDX<sub>I</sub>, NMDX<sub>II</sub>, NMD<sub>I</sub>, NMD<sub>XI-I</sub>, NMD<sub>XII-II</sub>, NMD<sub>L-IV</sub>, NMD<sub>XI-IV</sub>, T<sub>avg</sub>90p, WD, WW, SDII, R10, R20, R95p, R99p). In a few cases, however, a statistically significant downward trend was found: HDD15.5 (heating degree-days expressing the energy needed to heat a building), ID (number of ice days), T<sub>avg</sub>10p (number of cold days), CD (number of cold and dry days), CW (number of cold and wet days).

Table 1.

Percentile thresholds of daily mean air temperature and daily sum of precipitation calculated on the basis of data from the Polish Polar Station Hornsund in 1981–2010.

Percentile thresholds	Daily mean air temperature [°C]	Daily sum of precipitation [Σ mm]
1 <sup>st</sup> percentile	-23.0	0.1
5 <sup>th</sup> percentile	-18.4	0.1
10 <sup>th</sup> percentile	-15.4	0.1
25 <sup>th</sup> percentile	-9.3	0.3
75 <sup>th</sup> percentile	3.2	2.7
90 <sup>th</sup> percentile	4.2	6.4
95 <sup>th</sup> percentile	5.1	9.6
99 <sup>th</sup> percentile	6.5	19.0

The estimates of trends and their statistical characteristics of the analyzed climatic variables are shown in Table 2. The trend was estimated using the modified Mann-Kendall method (Hamed and Rao 1998) taking into account autocorrelation of the time series.

**Indices based on air temperature.** — Figure 4 shows the variability of freezing degree-days (FDD), thawing/positive degree days (TDD/PDD), warm season length (WSL<sub>0</sub>), the number of icing days (ID), the number of frost days (FD), the number of warm days (T<sub>avg</sub>90p) and the number of cold days (T<sub>avg</sub>10p) between 1979–2019. FDD was calculated for the hydrological year from 1 September to 31 August after Christiansen *et al.* (2013), as were PDD, also known as TTD, and WSL<sub>0</sub>. These indices describe the conditions of frozen ground as well as glacier melting and thawing of the active permafrost layer (Braithwaite 1995; Hock 2003; Frauenfeld *et al.* 2007; Christiansen *et al.* 2013). The mean long-term value of FDD, calculated for the hydrological year, is -1765.3°C and varied from -812.4°C in 2016 to -2910.3°C in 1981. A statistically significant decreasing trend was estimated with a slope of 325° C/decade. By contrast, the amount of heat, represented by PDD with a long-term



Table 2.

Variability of the indices between 1979–2019, including mean, standard deviation, maximum, minimum and slope of trend estimates. Statistically significant trends at the 0.05 level are indicated in bold.

Indicator	MEAN 1979– 2019	STD 1979– 2019	MAX 1979– 2019	MIN 1979– 2019	Linear trend /10yrs	Sen's Slope /10yrs	p-value
NDD	-1763.2	546.7	-500.3	-2990.3	367.828	368.295	1.08E-08
FDD	-1765.3	490.1	-812.4	-2910.3	324.990	325.022	4.36E-09
PDD	455.1	106.0	798.3	206.0	70.652	60.306	9.76E-05
WSL <sub>0</sub>	126.2	17.7	175.0	86.0	12.527	11.667	1.20E-05
GSL <sub>5</sub>	12.1	14.9	54.0	0.0	5.686	2.457	8.45E-02
sumT <sub>5</sub>	143.9	92.8	404.4	5.3	32.048	15.337	1.11E-01
GDD5	72.2	60.8	244.4	0.3	3.616	1.843	4.56E-02
HDD <sub>15.5</sub>	6987.3	591.1	8247.6	5552.1	-395.752	-403.873	2.98E-07
FD	32.6	6.5	48.0	20.0	1.331	1.607	5.20E-02
ID	177.4	28.6	276.0	107.0	-15.890	-15.071	1.45E-06
NMD <sub>XI</sub>	9.8	6.5	27.0	0.0	2.058	2.165	1.01E-02
NMD <sub>XII</sub>	7.0	5.4	22.0	0.0	1.936	2.407	8.50E-04
NMD <sub>I</sub>	6.0	5.1	21.0	0.0	1.976	1.667	8.30E-03
NMD <sub>II</sub>	4.9	4.6	21.0	0.0	1.336	0.833	8.17E-02
NMD <sub>III</sub>	4.9	4.4	15.0	0.0	0.186	0.000	9.82E-01
NMD <sub>IV</sub>	5.9	4.9	23.0	0.0	1.153	0.909	1.45E-01
NMD <sub>XI-I</sub>	23.1	12.7	53.0	3.0	6.498	7.029	1.92E-07
NMD <sub>XII-II</sub>	18.2	11.4	44.0	3.0	5.654	5.556	5.39E-05
NMD <sub>I-IV</sub>	21.7	11.3	50.0	1.0	4.652	4.422	8.09E-04
NMD <sub>XI-IV</sub>	39.1	16.5	82.0	9.0	8.967	10.000	1.62E-04
T <sub>avg</sub> 90p	42.5	19.5	94.0	2.0	10.531	9.428	1.71E-06
T <sub>avg</sub> 10p	32.6	22.1	91.0	1.0	-13.774	-14.031	1.99E-07
CD cold/dry days	70.0	24.1	126.0	16.0	-13.331	-13.333	0.00E+0
CW cold/wet days	1.9	1.9	8.0	0.0	-0.763	-0.625	1.19E-02
WD warm/dry days	38.8	12.4	68.0	8.0	5.871	5.714	8.22E-05
WW warm/wet days	15.4	8.6	42.0	1.0	3.639	2.753	2.61E-03
RR1 Wet days	85.7	16.2	125.0	58.0	2.704	2.727	2.86E-01
SDII Simple daily intensity index	5.0	0.8	6.3	3.5	0.397	0.444	1.68E-04
R10	10.7	4.3	20.0	3.0	1.822	2.000	1.22E-03
R20	2.5	2.3	8.0	0.0	1.040	0.833	4.98E-04
R75p No of moderate wet days	45.9	10.5	75.0	21.0	3.185	2.727	5.77E-02
R95p No of very wet days	11.2	4.5	23.0	3.0	1.948	2.083	1.27E-03
R99p No of extremely wet days	2.7	2.4	8.0	0.0	1.054	0.896	5.64E-04

annual mean of 455.1°C, increased at a rate of 70.6°C/decade for the linear trend or 60°C/decade for Sen's slope and varied from 206.0°C in 1982 to 798.3°C in 2016. The average duration of the WSL<sub>0</sub> (with T<sub>avg</sub> >0°C) was 125.0 days but fluctuated between 68 days (1982) and 194 days (2016), which represents

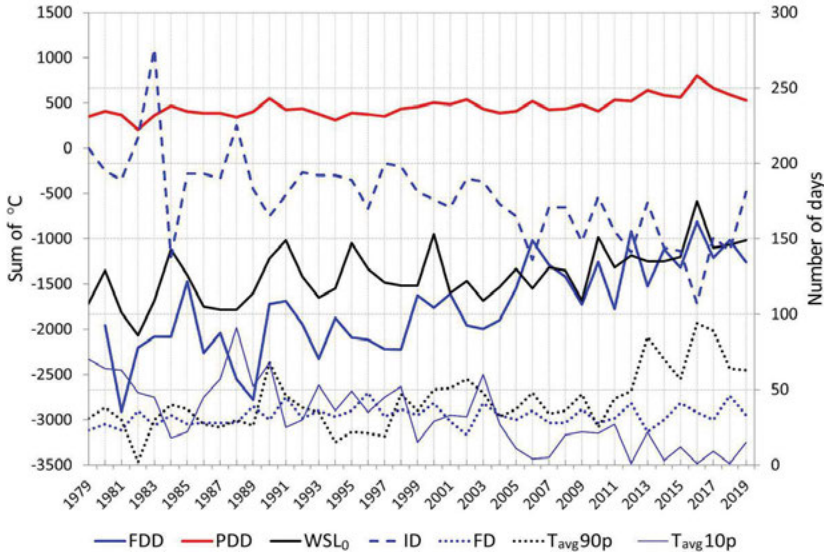


Fig. 4. Freezing degree-days (FDD), thawing/positive degree days (TDD/PDD), warm season length ( $WSL_0$ ), number of icing days (ID), number of frost days (FD), number of warm days ( $T_{avg90p}$ ) and number of cold days ( $T_{avg10p}$ ) during 1979–2019 at Hornsund. The Sums of FDD and PDD are shown on the left-hand y axis, whereas the right-hand y axis represents the number of days of other indices.

a difference in duration of *ca.* 3 months. A statistically significant increasing trend was found for  $WSL_0$  with slope 12.5 or 11.7 days/decade for the linear trend or Sen's slope, respectively.

The progressive warming has led to changes in the number of days with a daily temperature  $<0^\circ\text{C}$  (ID) to decrease at a rate of 15.8 days per decade between 1979–2019 with a non-significant increase in the number of frost days (FD). This effect is also expressed in an increase in the number of warm days with a  $T_{avg} >90^{\text{th}}$  percentile of the daily mean temperature ( $T_{avg90p}$ ) and a decrease in the number of cold days ( $T_{avg10p}$ ), described as days with a  $T_{avg} <10^{\text{th}}$  percentile of the daily mean temperature (Fig. 4, Supplementary tables 1 and 2).

Progressive warming, especially the rise in winter temperatures, must result in an increase in the number of thaws, as a result of which ice and icy layers are formed on the surface. Winter thaws in the Arctic are often identified as rain-on-snow events (Rennert *et al.* 2009; Bokhorst *et al.* 2016). The number of melting days (NMD, days with  $T_{max} \geq 0^\circ\text{C}$ ) from November to April was used to examine the episodes when snow cover thawed during winter (Fig. 5).

The large numbers of thaws that occur during the polar night and winter season are a consequence of the frequent advection of warm air masses during winter and highlight the oceanic nature of the region's climate. In the history of measurements, four episodes with mean monthly temperatures  $>-1^\circ\text{C}$  occurred in these months, including one with a temperature  $>0^\circ\text{C}$ : April 2006 ( $-0.3^\circ\text{C}$ ),

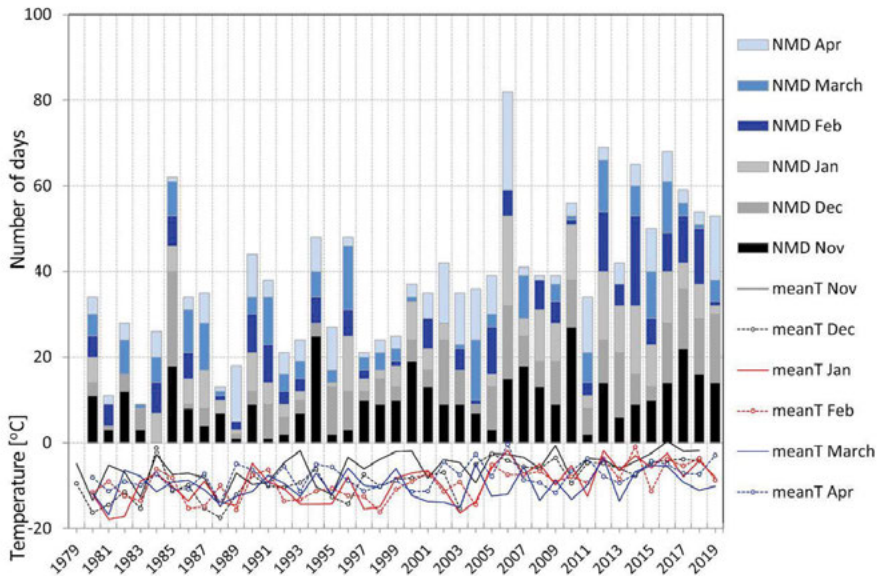


Fig. 5. The number of melting days (NMD, days with  $T_{\max} \geq 0^{\circ}\text{C}$ ) and monthly mean air temperature (meanT) from November to April in the winter seasons 1979–2019 in Hornsund.

November 2009 ( $-0.6^{\circ}\text{C}$ ), February 2014 ( $-0.9^{\circ}\text{C}$ ) and a very warm November 2016 with mean temperature of  $+0.4^{\circ}\text{C}$ . However, thaws occurring between November and April were recorded in all years for which measurements are available. The mean duration was 39.1 days over the entire period analyzed. The lowest number of days with thawing episodes (9) was recorded in the 1982/1983 season, while the highest number of thaw episodes occurred in the winter of 2005/2006, when maximum daily temperatures of  $\geq 0^{\circ}\text{C}$  were recorded on 82 days. Record high temperatures for January and April were recorded in that winter. The number of thaw episodes increased significantly in frequency after 2000. The trend analyses for this time series indicated a statistically significant trend ( $p$  value  $1.62\text{e-}04$ ) with a slope of 8.967 days/decade for the linear trend and 10.000 days/decade for Sen's method.

**Indices based on temperature and precipitation.** — Among the temperature- and precipitation-based indices, there was a greater frequency of both cold/dry days (CD) and warm/dry days (WD) followed by cold/wet (CW) and warm/wet (WW) days. The mean annual number of such days was 70 CD, 38.8 WD, 1.9 CW and 15.4 WW. A distinct, statistically significant downward trend with a rate of  $-13.3$  days per decade was recorded for cold/dry days. Cold days were distinguished from warm days by values below the 25<sup>th</sup> percentile and above the 75<sup>th</sup> percentile of the daily mean temperature. For dry days, the criterion was the threshold determined by values  $<25^{\text{th}}$  percentile of the total daily precipitation and for wet days the threshold was determined by values  $>75^{\text{th}}$  percentile of the total daily precipitation. If the number of wet days (RR1) is

treated as an index for counting days with precipitation  $\geq 1$  mm, there were on average 85.7 such days in a year. According to this criterion, the lowest number of such days (58) occurred in 1987 and the highest in 2016, when there were 125 days with precipitation  $\geq 1$  mm and also the lowest number of cold/dry days.

Two variables, *i.e.*, the number of days with precipitation  $R \geq 1$  mm (RR1 number of wet days) and SDII (Simple daily intensity index, mm/wet day), give a good indication of whether a given year was a season with abundant precipitation or was a deficit season. On average, there were 85.7 days per year with  $R \geq 1$  mm (wet days) and the SDII, computed by calculating the total precipitation on wet days divided by the number of wet days in the period, yielded an average daily precipitation of 5.0 mm for each wet day. The highest number of wet days (125) was recorded in 2016. The lowest number of wet days (58 cases) was recorded twice, in 1987 and 2019, when the annual precipitation was 230.2 mm and 264.5 mm, respectively. The highest SDII value of 6.3 mm/day was recorded in 1999, when the annual precipitation was only 68.6 mm higher than the multi-year mean value of 531.3 mm with an RR1 of 80 days. The lowest SDII of 3.5 mm/day was recorded in 1979 with precipitation that was not very abundant (260.3 mm), with 65 days with precipitation  $\geq 1$  mm. The picture that emerges from this analysis is that the wettest year, with the most abundant precipitation, was 2016, whereas 1987, 2019 and 1979 were extremely dry years. This is well illustrated by the annual SPI and SPEI, which were +2.38 and +2.29 in 2016 (moderately wet), 2.43 and 2.31 in 1987 as well as -1.98 and -2.34 in 2019 (moderately dry).

The number of days with extreme precipitation was determined by two methods. The first was used to determine the number of heavy precipitation days as days with daily precipitation  $\geq 20$  mm (RR20). The second method was used to determine the number of extremely wet days, assuming that those were days with precipitation  $>99^{\text{th}}$  percentile of the daily amounts. The latter approach is preferable because the statistically defined threshold is objective for all conditions. The threshold of the  $99^{\text{th}}$  percentile of total daily precipitation in the case of the climatic normal 1981–2010 is 19.0 mm. The difference in determining the number of days is that across the 1979–2019 data population, there were 111 days with precipitation  $>19.0$  mm (2.7 days per year on average) and slightly fewer, *i.e.*, 102 days with precipitation  $\geq 20$  mm (2.5 per year on average). Table 3 lists the characteristics of the occurrence of daily precipitation totals  $\geq 20$  mm, which averaged 29.2 mm in 1979–2019. However, there were dramatic records, such as the precipitation recorded on 18 September 2017, when the total amount was 73.5 mm, or the three consecutive days of 7–9 November 2016 with a total precipitation of 130.6 mm. The history of measurements at Hornsund indicates that the greatest number of extreme precipitation events occurred in September (27 days), October (22 days) and July (18 days). The highest number of days with extreme precipitation (8) was recorded in 2011, with 3 days in September and 3 in October.

Table 3.

The number of daily precipitation events  $\geq 20\text{mm}$  (RR20) with total precipitation ( $\Sigma R$ ) and mean precipitation per case ( $\Sigma R/\text{case}$ ).

	Jan	Feb	March	Apr	May	Jun	Jul	Aug	Sept	Oct	Nov	Dec	Num- ber of cases	$\Sigma R$	$\Sigma R/\text{case}$
1979															
1980									1 / 21.9	1 / 21.4			2	43.3	21.7
1981															
1982				1 / 34.5				1 / 22.6					2	57.1	28.6
1983			1 / 20.6			1 / 25.8							2	46.4	23.2
1984															
1985															
1986							1 / 40.5						1	40.5	40.5
1987															
1988							1 / 20.3						1	20.3	20.3
1989								1 / 31.7					1	31.7	31.7
1990								1 / 33.4	1 / 43.6				2	77.0	38.5
1991															
1992						1 / 26.0							1	26.0	26.0
1993									1 / 26.8				1	26.8	26.8
1994						1 / 25.1	1 / 33.1	1 / 58.3	1 / 38.2	2 / 46.1			6	200.8	33.5
1995												2 / 76.1	2	76.1	38.1
1996						1 / 20.2	1 / 25.3	1 / 22.0	2 / 85.6				5	153.1	30.6
1997															
1998										1 / 27.1			1	27.1	27.1
1999								2 / 59.8	4 / 106.1	1 / 20.5			7	186.4	26.6

	Jan	Feb	March	Apr	May	Jun	Jul	Aug	Sept	Oct	Nov	Dec	Num- ber of cases	$\Sigma R$	$\Sigma R /$ case
2000								1 / 26.7		2 / 53.7			3	80.4	26.8
2001									1 / 43.9				1	43.9	43.9
2002												1 / 20.2	1	20.2	20.2
2003															
2004			1 / 30.3	1 / 25.2			1 / 20.3	2 / 52.9	1 / 22.7	1 / 24.2			7	175.6	25.1
2005		1 / 20.3					1 / 25.4						2	45.7	22.9
2006					1 / 35.3	1 / 20.2							2	55.5	27.8
2007									1 / 24.7				1	24.7	24.7
2008								1 / 26.8	2 / 53.5				3	80.3	26.8
2009									1 / 24.5	3 / 66.6	2 / 48.0		6	139.1	23.2
2010	2 / 43.1						1 / 25.2			1 / 23.2			4	91.5	22.9
2011		1 / 21.4			1 / 20.8				3 / 75.2	3 / 72.9			8	190.3	23.8
2012							1 / 21.3	2 / 57.2	1 / 59.8				4	138.3	34.6
2013	1 / 28.5							2 / 58.1	1 / 21.8				4	108.4	27.1
2014									1 / 33.1	1 / 25.9			2	59.0	29.5
2015		1 / 23.1						1 / 49.8	4 / 123.8	1 / 22.7			7	219.4	31.3
2016										2 / 60.5	3 / 130.6		5	191.1	38.2
2017									1 / 73.5	1 / 37.8			2	111.3	55.7
2018				1 / 22.7			1 / 36.2	1 / 28.9		2 / 46.8	1 / 25.2		6	159.8	26.6
2019								1 / 29.1					1	29.1	29.1
Cases cases	3	3	2	3	2	5	9	18	27	22	6	3			
$\Sigma R$	71.6	64.8	50.9	82.4	56.1	117.3	247.6	557.3	878.7	549.4	203.8	96.3			
$\Sigma R /$ case	23.8	21.6	25.5	27.5	28.1	23.5	27.5	31.0	32.5	25.0	34.0	32.1			29.2

**Drought indices.** — The Standardized Precipitation Index (SPI), recommended by the WMO (2012), defines the deficit or excess of precipitation as standard deviations from long-term averages in terms of extremely/severely/moderately and near-normal dry or wet. The Standardized Precipitation Evapotranspiration Index (SPEI) developed by Vicente-Serrano *et al.* (2010), is the extended variant of SPI and explains climatic anomalies of the climatic water balance, *i.e.*, precipitation minus potential evapotranspiration. The differences between the SPI and SPEI values are small and do not affect the quality of drought conditions assessment in the study area (Fig. 6).

The changes in the drought conditions were quantified on the basis of trend analysis using the modified Mann-Kendall method. These outcomes are listed in Table 4. Statistically significant changes were estimated for the annual, May–

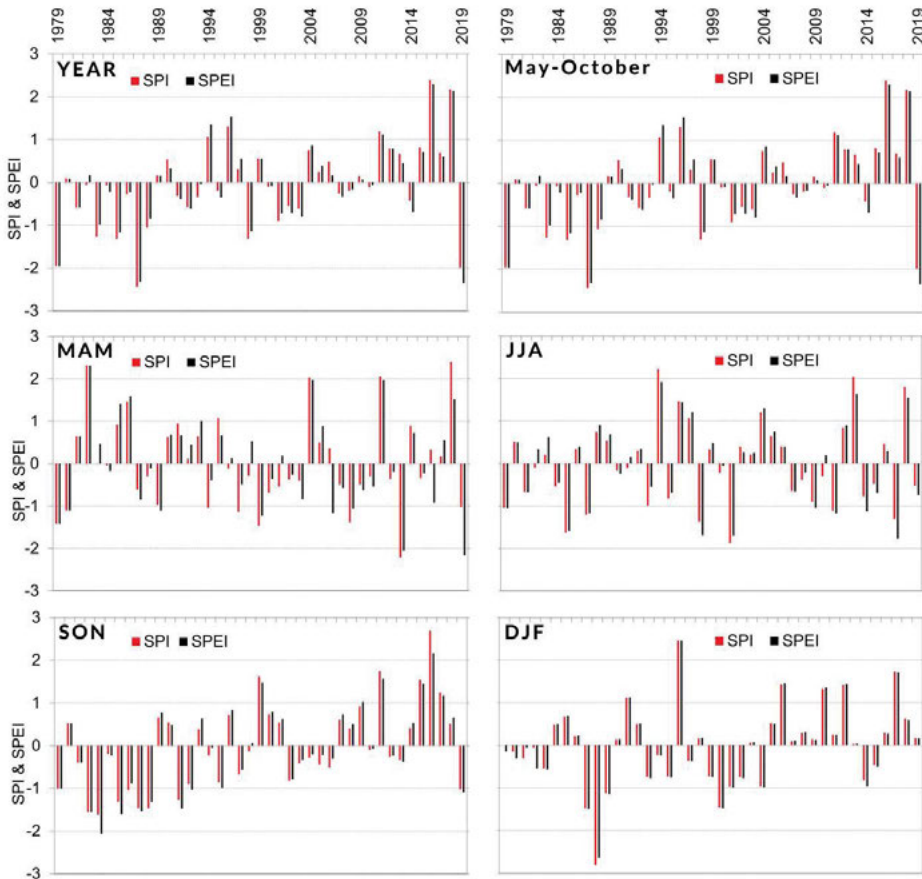


Fig. 6. Standardized Precipitation Index (SPI) and Standardized Precipitation Evapotranspiration Index (SPEI) in 1979–2019 at Hornsund for annual, May–October and quarter seasons: MAM, JJA, SON and DJF. Drought classes (DC): moderately wet  $2 < DC \leq 3$ ; slightly wet  $1 < DC \leq 2$ ; incipient wet spell  $0,5 < DC \leq 1$ ; near normal  $-0,5 \leq DC \leq 0,5$ ; incipient dry spell  $-0,5 > DC \geq -1$ ; slightly dry  $-1 > DC \geq -2$ ; moderately dry  $-2 > DC \geq -3$ .

Table 4.

The results of trend analysis using the modified Mann-Kendall method for Standardized Precipitation Index (SPI) and Standardized Precipitation Evapotranspiration Index (SPEI). Abbreviations as in Fig. 6.

	SPI		SPEI	
	Slope of trend	p-value	Slope of trend	p-value
annually	0.404	3.02E-03	0.337	3.99E-05
May–Oct	0.403	4.83E-10	0.358	1.57E-02
MAM	−0.028	8.49E-01	−0.186	2.96E-01
JJA	0.051	6.78E-01	−0.037	7.62E-01
SON	0.446	8.85E-04	0.501	1.78E-06
DJF	0.184	8.46E-02	0.178	9.20E-02

October and autumn (SON) scales for SPI and SPEI. The largest changes were obtained for SON, when negative SPI and SPEI occurred more often in the first part of the period and positive values dominated in the last 20 years.

On the basis of the annual and the warm half-year (May–October) data, a trend towards more frequent wet seasons becomes noticeable after 2010. This is particularly pronounced in the autumn quarter (SON), which in the 1980s was classified as slightly dry and in recent years as slightly wet and even moderately wet, although with the most recent 2019 season it was regarded as near-normal. SPI and SPEI for the SON quarter are consistent with the previous assessment, indicating that the greatest number of extreme precipitation events occurred in September (27 days) and October (22 days), and that their frequency was the highest in the last decade. Both SPI and SPEI and the previously mentioned values of RR1 and SDII confirmed that the wettest year with the most abundant precipitation was 2016, whereas the extremely dry years were 1979, 1987 and 2019.

The drought SPI and SPEI indices did not differ much with regard to the calculated drought deficits in the study area. During 1979–2019, there were 26.8% dry seasons and 31.7% wet ones according to SPI, but 31.7% dry seasons and 26.8% wet ones according to SPEI. The largest number of water deficit seasons occurred in the summer quarter (JJA), both indices being equal to 36.6%. The autumn quarter (SON) stood out as the most frequently "wet" one with 34.1% of cases according to SPI and 39.0% according to SPEI.

## Discussion

**Impact of pluviothermic conditions on glaciers and permafrost.** — It has been assumed that, despite local topoclimatic differences, the long-term series of measurements carried out in 1979–2019 at the PPS Hornsund reflect the weather



conditions and their environmental consequences in the W and SW coastal part of Wedel Jarlsberg Land (Migąła *et al.* 2013; Arażny *et al.* 2018). The tendency of pluviothermal conditions observed since the end of the 1950s in the Hornsund region is strongly correlated with the changes observed all over Svalbard. However, it is difficult to distinguish between the cold period (the second half of the 20<sup>th</sup> century) and the warm period since 1999 for the Hornsund data series (Nordli *et al.* 2020). Since the middle of the 20<sup>th</sup> century, an increasing trend in air temperature has been observed in Hornsund. Climatic conditions undoubtedly influence the glacier's intense recession, changing this important landscape element and heat balance of the area (Błaszczuk *et al.* 2013).

The glaciers on Svalbard have been losing mass since the 1960s, with a tendency towards a more negative mass balance since 2000 (Schuler *et al.* 2020). The warming and increase in PDD values together with the prolongation of the warm season is intensifying the ablation of glaciers and meltwater runoff. This is especially important in the case of glaciers terminating on land, such as Werenskioldbreen, situated 12 km NW of the PPS, where weight loss is due entirely to summer surface ablation (Bs). However, summer ablation is also playing a significant part in weight loss by tidewater glaciers. The average summer surface ablation of the Hornsund fjord glaciers in 2006–2015 was 40% of the total glacier mass loss (Błaszczuk *et al.* 2019). The positions of these glaciers are available at <https://toposvalbard.npolar.no/?lat=77.07001&long=15.64122&zoom=6&layer=map>.

Grabiec *et al.* (2012) used monthly values of air temperature and precipitation from the PPS meteorological station and reanalysis of ERA-40 data to hindcast the mass balance of Werenskioldbreen. A summary of summer surface ablation data from modelling (1979–2002) and observations (1999–2019) shows an increase in the average 10-year surface ablation from  $-1.16$  m w.e. in 1979–1988, through  $-1.35$  and  $-1.55$  m w.e. in 1989–1998 and 1999–2008, respectively, to  $-1.67$  m w.e. in 2009–2018. The average increase in Werenskioldbreen summer surface ablation in 1979–2018 was  $0.13$  m w.e. per decade. The Hansbreen tidewater glacier, adjoining Werenskioldbreen, showed a similar growth trend in average summer surface ablation per decade from  $-1.22$  m w.e. in 1989–1998 to  $-1.35$  and  $-1.47$  m w.e. in 1999–2008 and 2009–2018, respectively (Fig. 7). The average increase in Hansbreen's surface summer ablation in 1989–2018 was  $0.08$  m w.e. per decade. The difference in the ablation trend is due to different glacier exposures and different conditions of snow accumulation, which affect summer surface ablation. However, the mean ablation rates for Werenskioldbreen and Hansbreen in 1989–2018 were similar at  $0.32$  and  $0.28$  m w.e. per 100 PDD, respectively. The slowing down of the ablation rate on both glaciers during the last decade is interesting, however (Table 5). It is most likely the effect of a prolonged ablation period induced by a greater number of days with positive air temperatures at the end of the ablation season. During this period, the average daily temperatures were still above zero, but ablation was minimal on the glacier

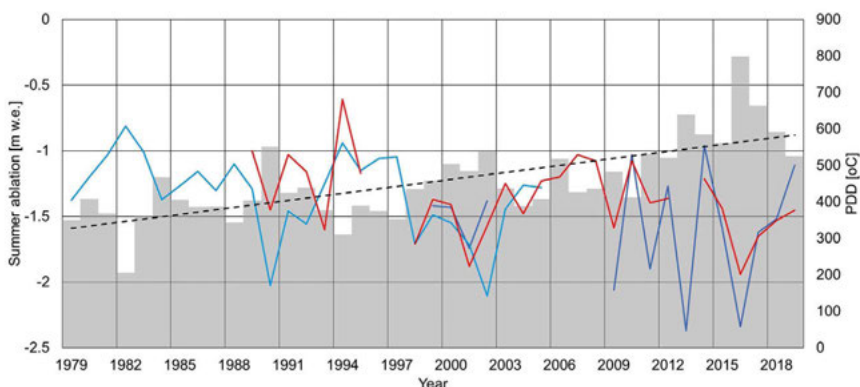


Fig. 7. Werenskioldbreen and Hansbreen summer surface ablation versus Positive Degree Days (PDD) between 1979–2019. Blue line – modelled summer ablation of Werenskioldbreen in 1979–2002 (Grabiec *et al.* 2012), dark blue line – summer ablation of Werenskioldbreen recorded in 1999–2002 and 2009–2019 (Ignatiuk *et al.* 2022), red line – summer ablation of Hansbreen recorded in 1989–2019 (WGMS), grey columns – PDD (Wawrzyniak and Osuch, 2020), black dashed line – linear trend of PDD.

Table 5.

Average summer surface ablation (Bs) and ablation rate of Werenskioldbreen and Hansbreen between 1979–2018 after Grabiec *et al.* (2012) and Ignatiuk *et al.* (2022).

Period	Avg. PDD	Werenskioldbreen		Hansbreen	
		Avg. Bs [m w.e.]	Avg. Ablation rate [m w.e. / 100 PDD]	Avg. Bs [m w.e.]	Avg. Ablation rate [m w.e. / 100 PDD]
1979–1988	368	-1.16	0.32	-	-
1989–1998	406	-1.35	0.33	-1.22	0.30
1999–2008	460	-1.55	0.34	-1.35	0.29
2009–2018	579	-1.67	0.29	-1.47	0.25

surface. The rate of ablation was also affected by the lower number of sunny days and the higher number of days with precipitation and cloud cover.

The calculations by Frauenfeld *et al.* (2007) for the entire Northern Hemisphere showed that from the 1970s to the end of the 20<sup>th</sup> century, FDD (freezing degree days – sum of  $T_{avg} < 0^{\circ}\text{C}$ ; freezing index) decreased at the rate of  $85.6^{\circ}\text{C}$  per decade, whereas PDD/TDD (positive degree days; thawing degree days – sum of  $T_{avg} > 0^{\circ}\text{C}$ ; thawing index) increased at a rate of  $44.4^{\circ}\text{C}$  per decade. The rate of decrease of FDD for the Hornsund area was almost four times faster at  $324.9$  per decade between 1979–2019 (Tables 1 and 2, Fig. 4). The increase in PDD/TDD was less dramatic at  $70.6$  per decade. Permafrost in Svalbard is the warmest in the Arctic, and future climate models predict a general warming of the Svalbard permafrost as well as permafrost degradation near the coasts at

altitudes below *ca.* 100 m a.s.l. in well-drained locations with dry bedrock and a potentially hazardous, irregular acceleration in the thawing of near-surface permafrost (Isaksen *et al.* 2007a, 2007b; Etzelmüller *et al.* 2011; Christiansen *et al.* 2013). The increase in total TDD/PDD and the duration of the warm season (WSL) indicate a warming of the permafrost and deeper thawing of the active layer. Etzelmüller *et al.* (2011) reported that in 2001–2010 the warming rate at the permafrost surface (*ca.* 2 m depth) was 0.07°C/year but that the rate of increase depended on the water content in the near-surface layers. A further increase in temperature since 2010 means that a deeper thawing of the active layer of the permafrost is occurring, which in turn is reflected by changes in the surface and subsurface hydrological conditions, the soil moisture balance and ecosystem productivity. Opała-Owczarek *et al.* (2018) pointed out that an increase in temperature during the growing season did not necessarily promote plant growth, indicating rather that drought stress caused by water table lowering was related to increasing thaw depths.

**Atmospheric circulation and extreme episodes of thermal conditions.** — The extreme TDD/PDD (thawing degree days/positive degree days) values that were recorded during the study period were 206.0°C in 1982 and 798.3°C in 2016. The record high PDD totals were influenced not only by warmer temperatures but also by the WSL<sub>0</sub> warm season duration (duration of the period with  $T_{\text{avg}} > 0^\circ\text{C}$ ), which in 2016 was twice as long (175 days) as the warm season in 1982 (86 days). Extreme FDD values (freezing degree days calculated for the hydrological year from 1 September to 31 August) were recorded in the 1980/1981 and 2015/2016 seasons with respective totals of –2910.3°C and –812.4°C. The frequency of atmospheric circulation types in the seasons with extreme sums of TDD/PDD and FDD indices is shown on Fig. 8.

The high PDD total in 2016 was associated with a *ca.* 40–42% larger share of both cyclonic and anticyclonic circulations from the S+SW sector than the multi-year mean, forcing the advection of warm air masses from the south, and a 25% increase in synoptic situations in which Spitsbergen was at the center of a low pressure area or at the edge of a trough of low pressure (Cc+Cb). The unfavourable heat stock recorded at Hornsund in 1982 was primarily the result of the greater influence of low-level circulation from the E+SE sector (Figs. 8 and 9). This circulation also activated a branch of the cold East Spitsbergen Current and contributed to the drift of an extensive sea ice field that spread along the west coast and filled the Hornsund fjord area. Isaksen *et al.* (2016) found a high and negative correlation between sea ice concentration and air temperature in the Svalbard region and stated that the atmospheric warming observed in this area was driven by heat exchange from the larger open water areas in the Barents Sea and the region north of West Spitsbergen.

The record total of negative daily air temperatures (FDD Freezing Degree Days) reached in winter 1980/81 was caused by the greater advection of cold air masses from the N+NE sector generated by anticyclonic situations and air inflow

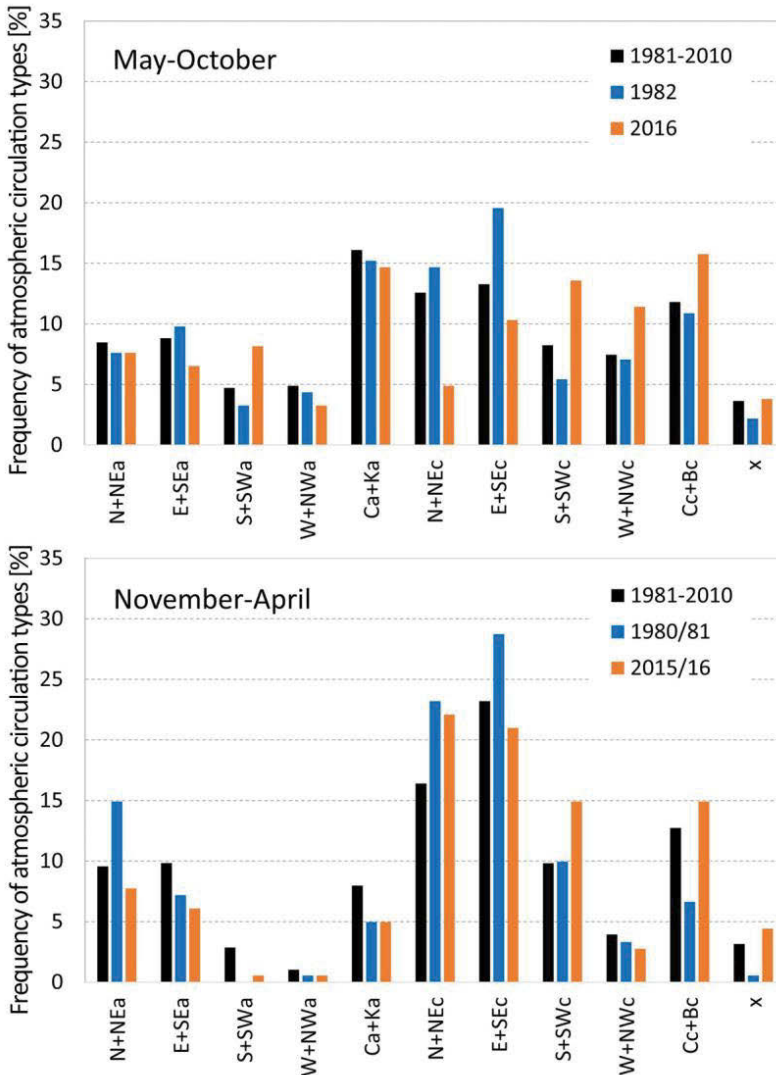


Fig. 8. The frequency of atmospheric circulation types (Niedźwiedź 2020) in seasons with extreme sums of Positive Degree Days /Thawing Degree Days TDD/PDD (left) and Negative Degree Days FDD (right) vs. climatic normal 1981–2010.

from the E+SE sector in cyclonic conditions than that resulting from the climatic normal frequency. During the 1980/81 winter quarter alone, Spitsbergen and NE Greenland were subject to strong negative air temperature anomalies. In turn, the exceptionally warm winter in 2016 with the lowest sum of negative temperatures was the result of an unusually high frequency of synoptic situations in which Spitsbergen was at the center of a low or a low pressure trough (Cc+Bc) and in situations with more frequent advection of air masses from the S+SW sector than the long-term mean, forced by low pressure areas. The synoptic conditions

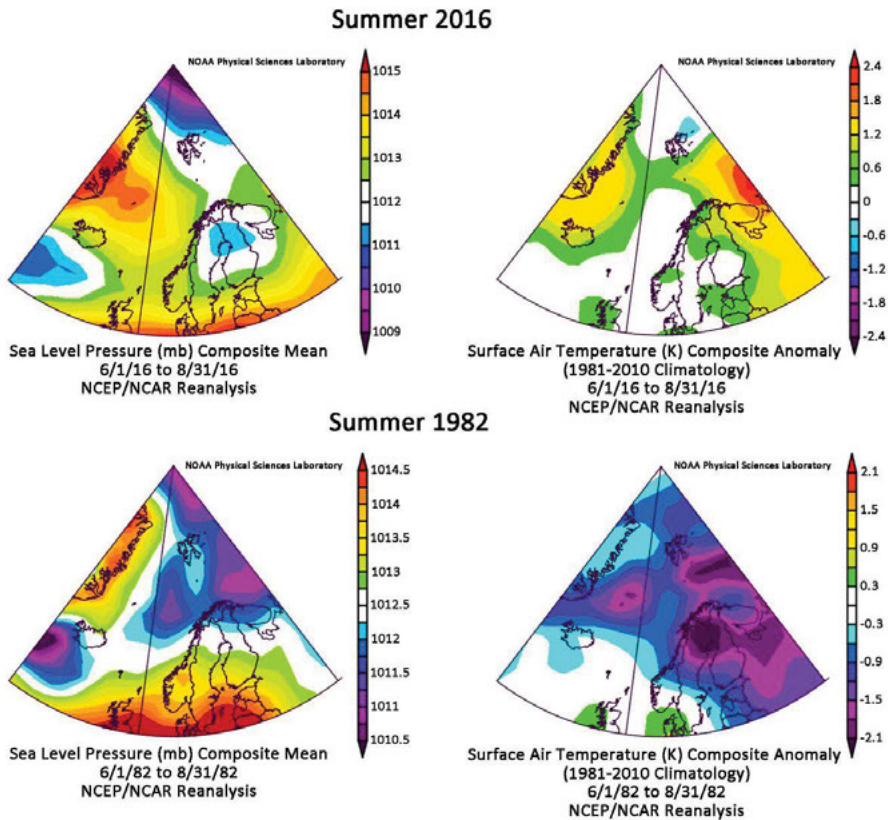


Fig. 9. Sea level atmospheric pressure (left) and air temperature anomaly (right) during seasons with extreme totals of Thawing/Positive Degree Days (TDD/PDD). Image provided by the NOAA/ESRL Physical Sciences Laboratory, Boulder, Colorado, from their website at <http://psl.noaa.gov> and submitted 26 May 2021.

resulted in the formation of positive temperature anomalies over the Spitsbergen area (Fig. 10).

The lowest air temperatures are related to air advection from the N and NE and, conversely, the highest temperatures are associated with air flows from the southerly sector during both cyclonic and anticyclonic conditions (Isaksen *et al.* 2016; Łupikasza and Niedźwiedź 2019). The direction of air mass advection and the frequency of pressure systems determining the weather in this area are well expressed by two indices, *i.e.*, the meridional, southerly index (S) and the cyclonicity index. The variability of the atmospheric circulation above Svalbard was studied by Niedźwiedź (2013a, 2013b), who concluded that the most significant influence on air temperature in particular seasons was exerted by the southerly, meridional index (S) of atmospheric circulation. A positive S index explains the inflow of warm air masses (advectations from the S, SW and SE), while a negative value represents the advection of cold air masses from the N, NW and NE. The impact of this index on air temperature is most pronounced in

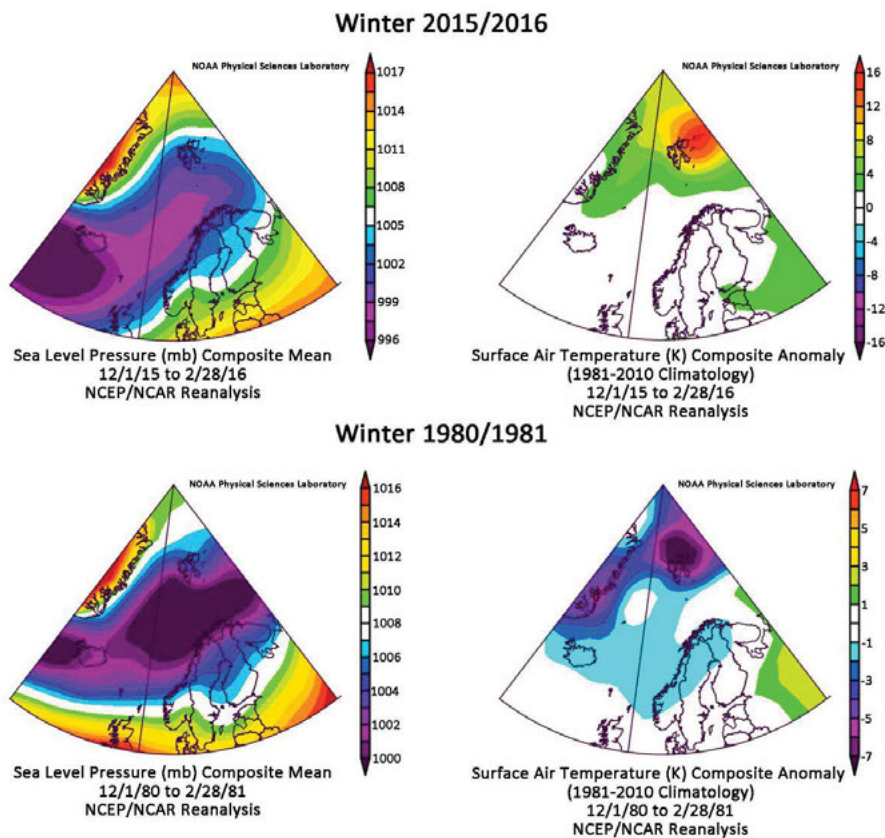


Fig. 10. Sea level atmospheric pressure (left) and air temperature anomaly (right) during seasons with extreme sums of Freezing Degree Days (FDD). Image provided by the NOAA/ESRL Physical Sciences Laboratory, Boulder, Colorado, from their website at <http://psl.noaa.gov> and submitted 26 May 2021.

autumn and winter, and the least in summer. The summer rise of the cyclonicity index, a positive value of which explains the predominance of cyclonic over anticyclonic situations, leads to a decrease in air temperature in summer, while causing warming in winter and spring.

Rising temperatures lead to a reduced fraction of solid precipitation. Łupikasza and Cielecka-Nowak (2020) analyzed the changing probabilities of days with snow and rain in the Atlantic sector of the Arctic. They found that the probability of days with liquid precipitation increased on an annual basis, from 1% to 2.9% per 10 years, strongly in September and October, between 1979 and 2017. No trend in the probability of liquid precipitation in the winter months was identified, but a negative trend of the probability of days with solid precipitation was found on an intra-annual scale at Hornsund in November, January and February. The present analysis indicates that the number of melting days (NMD, days with  $T_{\max} \geq 0^{\circ}\text{C}$ ) during the November–April period has increased since

2000, which is in accordance with the results of Łupikasza *et al.* (2019), who stated that the totals and frequency of winter rain have also increased significantly since 2000. The episode with the maximum number of 82 days with a maximum temperature  $\geq 0^{\circ}\text{C}$ , recorded in the winter of 2005/2006, was due to the northerly advection of oceanic heat with Atlantic Water (AW) and changes in the properties of the West Spitsbergen Current, which have influenced the local climate conditions in the Fram Strait region. Oceanographic research conducted in 2000–2007 by Walczowski and Piechura (2011) showed that in 2005–2006 there was an intensification of heat transport by AW. The authors noted a strong correlation between the interannual changes of the mean AW summer temperature from  $2.1^{\circ}\text{C}$  to  $3.7^{\circ}\text{C}$  and changes in the mean annual air temperatures at Hornsund from  $-5^{\circ}\text{C}$  to  $-1.5^{\circ}\text{C}$ . Isaksen *et al.* (2007a) reported that the thermal response of this episode was detectable to a depth of at least 15 m and stated that the greater frequency of high-temperature anomalies in the future would cause a potentially hazardous acceleration of permafrost thawing.

Winter thaws in the Arctic are often described as "rain-on-snow events" (ROS), with negative consequences for the functioning of polar ecosystems. Rennert *et al.* (2009) reported that ROS events, *i.e.*, the formation of icy layers, hampered the functioning of mammals during winter, whose populations fell as a result of restricted access to food. Bokhorst *et al.* (2016) and Opała-Owczarek *et al.* (2018) indicated a strong impact of ROS on vegetation through the eroding effects of snow blizzards on ice-covered tundra. Łupikasza *et al.* (2019) found that an increase in the frequency of ROS events impacted both glacier mass balance and glacier dynamics and concluded that the total liquid precipitation during winter could be effectively stored in the glacier, contributing 9% of the seasonal snow cover accumulation as a component of the glacier mass balance. Wickstrom *et al.* (2020) drew attention to the fact that winter ROS events occurred predominantly in an atmospheric circulation forcing the advection of southerly air masses during the passage of a low pressure center/trough and that the largest spatial extension of melting episodes and ROS events was from the SW. Climate models show that many parts of the Arctic will become vulnerable to ROS over the next 50 years (Rennert *et al.* 2009).

**Atmospheric circulation and extreme episodes of precipitation.** — Increasing precipitation in the Arctic in the past century has been reported in several studies, a trend that has also been identified for the Svalbard area (Førland *et al.* 2011; Walsh *et al.* 2020). Attention is drawn to the fact that the observed positive trend in precipitation is false because of the annual correction factor and that the real increase of precipitation estimated for Svalbard Airport is 1.7% per decade, compared with earlier calculations for the period 1964–1997 that indicated 2.9% per decade (Førland *et al.* 2000, 2002).

Changes in the precipitation phase in the climate models run by Landrum and Holland (2020) indicate that the length of the rainy season (liquid phase) is increasing and its duration over the Arctic Ocean is increasing more dramatically

than over continental regions. The RCP8.5 scenario shows that by the end of the 21<sup>st</sup> century there will be Arctic regions where rain can occur in any month of the year. Very-wet-day precipitation as well as the number of days with heavy precipitation are also projected to increase (Walsh *et al.* 2020).

Extremes are becoming routine in the Arctic (Landrum and Holland 2020). This tendency is expressed, among other things, by the frequency of days with heavy precipitation, which has exhibited a significantly increasing trend in large parts of the northern high latitudes (Walsh *et al.* 2020). Serreze *et al.* (2015) found that in the case of Svalbard, extreme precipitation events showed no systematic temporal trend between 1979 and the early 2000s.

Two specific precipitation values were recorded at Hornsund during the 1979–2019 period. The highest ever measured daily total of 73.5 mm occurred on 19 September 2017 and unusually heavy precipitation (a total of 130.6 mm) occurred on 8–10 November 2016. This precipitation accounted for 15.9% and 28.2% of the mean annual totals, respectively, and occurred under synoptic conditions regarded as typical of extreme precipitation situations in the area. Serreze *et al.* (2015) stated that extreme events tended to occur when the region was influenced by a trough of low sea level pressure extending from the SW but that some of the largest precipitation events could be associated with a 500 hPa anomaly of geopotential height, *i.e.*, positive over the Barents Sea and negative over Greenland, and positive anomalies in precipitable water with a stream extending up to thousands of kilometres southwards into the subtropical Atlantic (Fig. 11). The situation forming these heavy rain episodes was in both cases elicited, using the classification of atmospheric circulation types proposed by Niedzwiedz (2013a, 2020), by the cyclonic type advection of air masses from the S+SW directions, that is from the sector with the highest probability of extreme rains.

The studies carried out by Niedzwiedz (2013a, 2013b) and Łupikasza and Niedzwiedz (2019) concluded that the increasing trend in the frequency of large precipitation events observed at Hornsund since 1994 was due to a greater frequency in the intensity of westerly and southerly atmospheric circulations, as expressed by the zonal and meridional circulation indices.

The observed increase in summer precipitation and heavy rain events can have a substantial impact on the characteristics of the snowpack, permafrost and activity of geomorphic processes (Owczarek *et al.* 2013; Hansen *et al.* 2014). Dendrochronological research of debris flow events, one of the most characteristic processes in non-glaciated areas in the Arctic, carried out in the vicinity of the Hornsund fjord, showed a clear relationship between heavy precipitation and increased mass movement activity. Wood anatomy features of *Salix polaris* and *Salix reticulata* sampled from debris flow tracks within debris cones located in the Fugleberget and Gullichsenfjelet foothills indicate an increase of debris flow activity from the 1990s onwards. The locations of these sites are available at <https://toposvalbard.npolar.no/?lat=77.07001&long=15.64122&zoom=6&layer=map>.



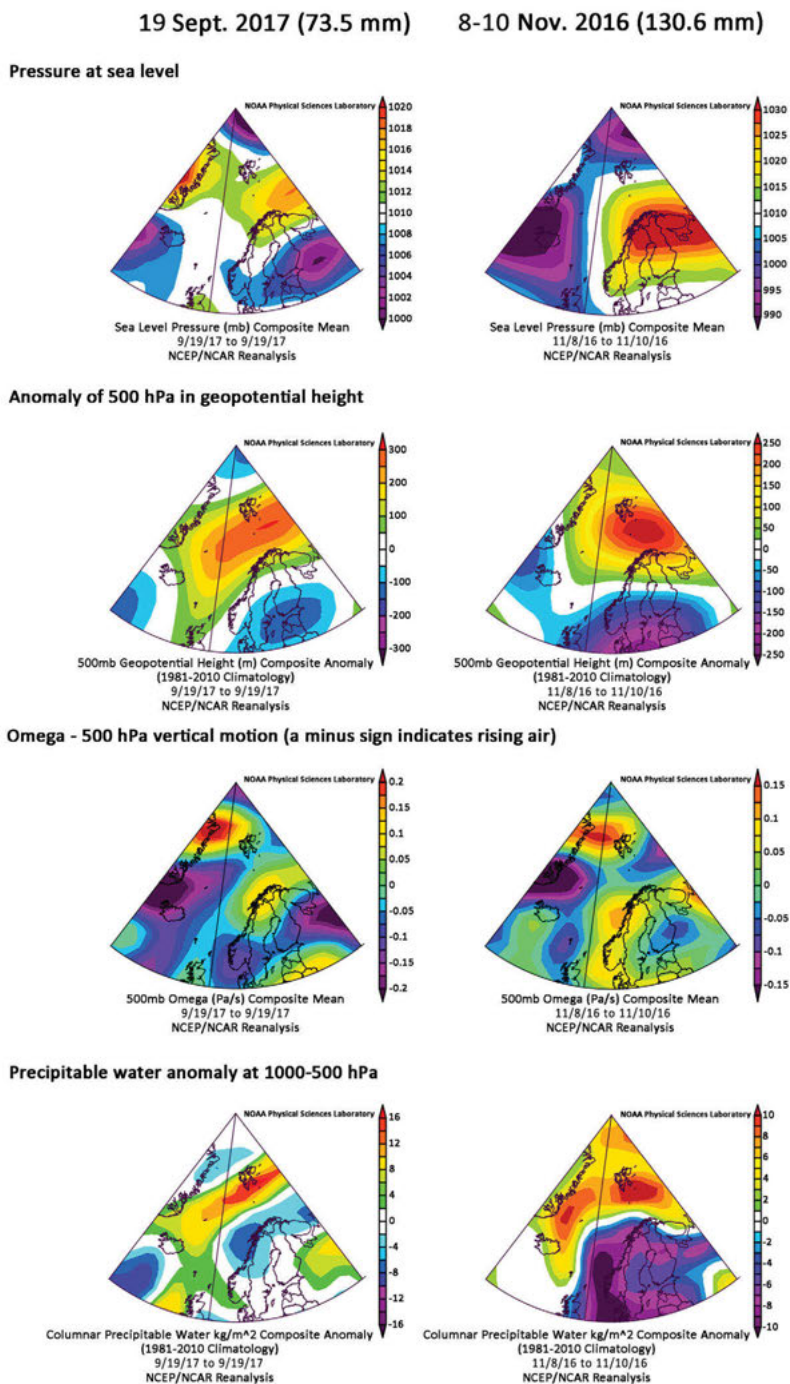


Fig. 11. Conditions in the atmosphere over the North Atlantic forming extreme precipitation events at Hornsund. Image provided by the NOAA/ESRL Physical Sciences Laboratory, Boulder, Colorado, from their website at <http://psl.noaa.gov> and submitted 26 May 2021.

A particular intensification of this process took place in 1994 and 1996 when large amounts of summer precipitation were recorded (Owczarek *et al.* 2013). Studies of debris flows in Svalbard and northern Scandinavia based on geomorphic and lichenometric analyses also indicate that this process can be correlated with extreme precipitation during summer (Larsson 1982; Rapp and Nyberg 1988; André 1995) rather than with snow melting in spring (Jahn 1976). However, it should be noted that extreme rainfall events are important as land-forming events during the year. The heavy precipitation episode noted in November 2016 triggered several landslides and slush flows in Svalbard that were identified by satellite imagery (Hanssen-Bauer *et al.* 2019). Similar hazardous events, which had previously impacted both snowpack and permafrost leading to the transformation of relief, were observed in the Ny-Ålesund area in January 2012 (Hansen *et al.* 2014), but such high amounts of precipitation were not recorded at that time at Hornsund.

An overall increase in air temperature and precipitation in the Arctic and high latitudes is reflected by the intensification of the hydrological cycle in glaciated and unglaciated catchments. The greater number of days with extreme precipitation >20 mm (R20), that have been recorded since the 1990s, has been reflected in an increase in floods driven by heavy rainfall events, see Supplementary table 2.

An increase in water discharge is apparent at a wide range of basin scales, *i.e.*, from small catchments (Lewis and Lamoureux 2010; Young *et al.* 2015; Stuefer *et al.* 2017) to large basins in North America (Déry *et al.* 2009; Yang *et al.* 2015) and Eurasia (Shiklomanov and Lammers 2009; Rawlins *et al.* 2010). The hydrological response to extreme meteorological events showed the increasing importance of summer/early autumn precipitation events in the generation of high discharges in the High Arctic (Lewis *et al.* 2012; Young *et al.* 2015; Stuefer *et al.* 2017), which eventually led to a switch from a nival to a pluvial type of hydrological regime in ice-free basins (Beel *et al.* 2018). Earlier initiation of snowmelt and a decrease of snowmelt in the annual runoff have been noted in multiple locations in the Arctic (Lewis *et al.* 2012; Young *et al.* 2015; Beel *et al.* 2018). However, a decrease in soil moisture as a consequence of warming leads to a lower response to rain events due to the water deficit (Favaro and Lamoureux 2014).

The situation in large catchments with a significant coverage of glaciers is slightly different. Here, the main supply of water is the melting snow and ice, but the hydrologically active season is getting longer (Nowak and Hodson 2013; Wawrzyniak and Osuch 2019), and it is influencing the water cycle in glaciated catchments (Nowak *et al.* 2021). For example, in the southern part of Svalbard the climatically driven changes are causing more frequent extreme rainfall events in late autumn and increasing the amount of rainwater in the total runoff (Majchrowska *et al.* 2015; Lepakowska and Stachnik 2018). These changes in the hydrological cycle in glaciated and unglaciated catchments are reflected in the

course of fluvial processes and the transformation of river channel patterns. An analysis conducted in two partly-glaciated basins in the Hornsund area (the Arie and Brattegg Rivers) has revealed an increase in lateral erosion processes and the rate of downcutting since the 1990s (Owczarek *et al.* 2014). The increasing significance of water input into river basins from rainfall is especially apparent in the river bed architecture. The wide channel bottoms that developed before the 1980s have been rapidly transformed into narrower ones. This is the main fluvial response to the increase in temperature and precipitation since the 1990s. The contraction of flow to a narrower zone leaving braid-plains behind is a response to the contemporary increase in the number and intensity of summer rainfall events. Extreme rainfall events generate flooding and remove the river bed sediment responsible for braiding. They are the main cause of the present incision of the Brattegg and Arie River channels (Owczarek *et al.* 2014).

**Atmospheric circulation and extreme episodes of drought conditions.** — The statement by Serreze *et al.* (2015) that extreme precipitation events depend on anomalies of geopotential and precipitable water determined by the baric field over the North Atlantic can be extended to explain the opposite situation relating to drought and its environmental consequences. Analysis of SPI and SPEI shows that the most seasons with a water deficit have occurred in the summer quarter (JJA), whereas the autumn quarter (SON) has been the most frequently identified as being wet. The forty-year history of weather conditions at Hornsund shows that there are indications of three episodes with extreme SPEI values. The driest were the summer quarters (JJA) in 2017, 2001 and 1998 with SPEI values of  $-1.76$ ,  $-1.69$  and  $-1.68$ , respectively. The wettest autumns (SON) were in 2016 (with SPEI 2.16), 2010 (1.56) and 1999 (1.48). The atmospheric conditions over the North Atlantic creating the most extreme drought conditions at Hornsund (both driest and wettest) are illustrated in Fig. 12.

Both extreme precipitation events and wet conditions, as expressed by high positive SPI and SPEI, depend on anomalies of geopotential and precipitable water determined by the baric field over the North Atlantic. By contrast, a deficit of atmospheric water and periods of dryness are expressed by negative drought indices. Situations like these take place over Svalbard when an area of high pressure develops over Greenland and the Barents Sea, blocking the transport of moisture usually associated with the cyclonic advection of air masses from the S+SW sector. Convection favoring extreme rainfall weakens under high pressure conditions, and the development of an anticyclone blocks the increase in precipitable water in the atmosphere, consequently inhibiting the formation of precipitation and reducing the amount of rain. The low pressure zone is then shifted to the south and extends along the trajectories of the atmospheric fronts moving latitudinally from Iceland towards Scandinavia. The positions of the lows are marked by the 500 hPa geopotential height anomalies.

Dry periods, *i.e.*, droughts, as well as excess precipitation, have a negative environmental impact. The drought episodes during summer do not promote

**Driest: SPEI JJA (-1.76) in 2017 Wettest: SPEI SON (2.16) in 2016**

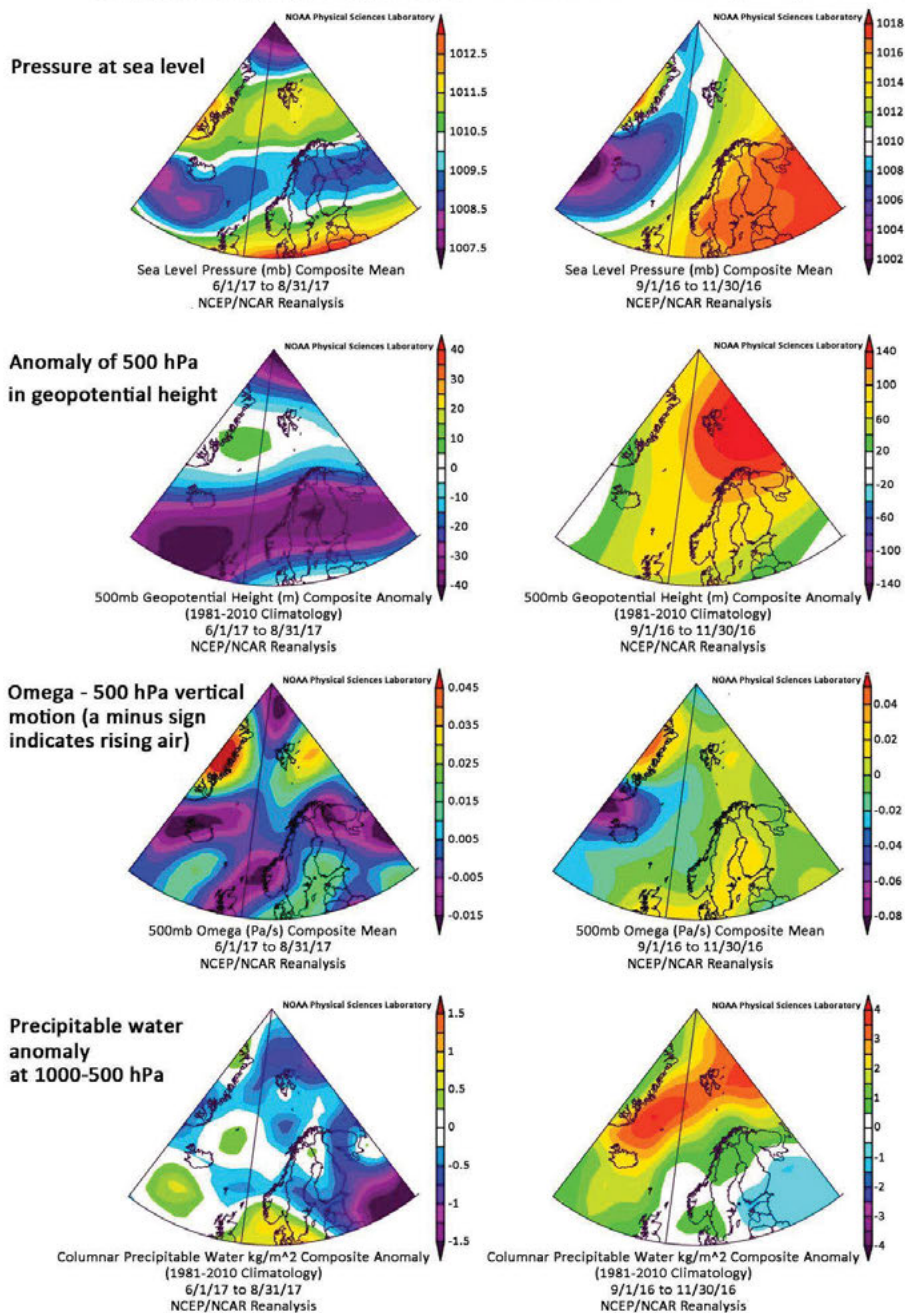


Fig. 12. Atmospheric conditions over the North Atlantic creating the most extreme drought conditions at Hornsund. Image provided by the NOAA/ESRL Physical Sciences Laboratory, Boulder, Colorado, from their website at <http://psl.noaa.gov> and submitted 26 May 2021.

plant growth and at the same time exacerbate the soil water deficiency caused by the lowering of the water table due to the increase in the thaw depth (Opała-Owczarek *et al.* 2018). With rising temperatures and summer PDD values, this is the second important factor which can inhibit plant growth or even kill vegetation, a process widely known as "tundra browning" (National Academies of Sciences, Engineering, and Medicine 2019). However, it should be noted that, because of the multiplicity and complexity of meteorological factors and extreme events, the causes of browning trends remain unclear (Phoenix and Bjerke 2016; Reichle *et al.* 2018).

## Conclusions

The data from Hornsund confirm the amplification of Arctic warming in the study area with a dramatic increase in annual temperature of  $+1.14^{\circ}\text{C}$  per decade in the last forty years (1979–2019) in SW Spitsbergen. During this period, this area's climate warmed more than six times more strongly than the global average that reached  $+0.17^{\circ}\text{C}$  per decade (NOAA 2020). Apart from the temperature increase, the annual increase in total precipitation (61.6 mm per decade) and the distinctive increases in precipitation in September and October of 19.67 mm and 13.53 mm per decade, respectively, show that evident changes have taken place. Climatic conditions undoubtedly influence the glacier's intense recession, changing this important landscape element and heat balance of the area.

The determined climate indicators work very well for tracking changes in the environment. The most dynamic are: (i) the cumulative sum of sub-zero temperatures that freeze the ground (FDD) decreased at a rate of  $324.9^{\circ}\text{C}$  per decade between 1979–2019; (ii) the heat supply expressed as PDD with a long-term annual mean of  $455.1^{\circ}\text{C}$  increased at a rate of  $70.6^{\circ}\text{C}$  and varied from  $206.0^{\circ}\text{C}$  in 1982 to  $798.3^{\circ}\text{C}$  in 2016; (iii) the number of melting days (NMD) occurring during the polar night and winter season indicates the frequent influence of warm air advection during winter and highlights the oceanic type of climate in the region, *i.e.*, during 1979–2019, thaws with an average of 39.1 days were recorded between November and April and their episodes increased significantly in frequency after 2000; (iv) more days with extreme precipitation  $>19$  mm have been noted in the study area since the 1990s, reflecting an increase in total runoff and floods driven by heavy rainfall events; (v) the rate of freezing index decrease for the Hornsund area is almost four times faster than for all the Northern Hemisphere, being equal to  $324.9$  per decade between 1979–2019, the increase in the thawing index (PDD/TDD) is less extreme at a rate of  $70.6$  per decade; (vi) the increase in positive degree-day totals (PDD) along with the prolongation of the warm season (WSLO), the rise in the number of melting days during winter (NMD), and the greater incidence of heavy rainfall have been observed; (vii) the mean ablation rates for glaciers situated in close proximity to

PPS Hornsund (Werenskioldbreen and Hansbreen) are similar: 0.32 m w.e. and 0.28 m w.e. per 100 PDD, respectively for 1989–2018. Trends in climatic variables reflected in numerous hydro- and bioclimatic indices have an impact on the dynamics of the High Arctic geoecosystem and characterize it very well.

**Acknowledgements.** — The results presented in this paper were obtained within Project No. 2017/27/B/ST10/01269 *Reconstructions and projections of the hydro-climatic conditions of southern Spitsbergen*, financed by the Polish National Science Centre. Glaciological data have been processed under assessment of the University of Silesia in Katowice data repository within the project Integrated Arctic Observing System (INTAROS, EU Horizon 2020, grant no. 727890) and Svalbard Integrated Arctic Earth Observing System – Knowledge Centre (Research Council of Norway, project no. 291644). The studies were carried out as part of the scientific activity of the Centre for Polar Studies (University of Silesia in Katowice) with the use of research and logistic equipment of the Polar Laboratory of the University of Silesia in Katowice. The authors would like to acknowledge Peter Senn for the linguistic proofreading and two anonymous reviewers for their constructive reviews.

## Supplementary materials

Supplementary table 1. Indices based on air temperature between 1979–2019, Polish Polar Station in Hornsund.

Supplementary table 2. Indices based on precipitation and air temperature between 1979–2019, Polish Polar Station in Hornsund.

Supplementary table 3. Drought indices (SPI and SPEI) between 1979–2019, Polish Polar Station in Hornsund.

## References

- Anderson J.N., Saros J.E., Bullard J.E. *et al.* 2017. The Arctic in the twenty-first century: Changing biogeochemical linkages across a paraglacial landscape of Greenland. *BioScience* 67: 118–133. doi: 10.1093/biosci/biw158.
- André M.F. 1995. Holocene climate fluctuations and geomorphic impact of extreme events in Svalbard. *Geografiska Annaler* 77A: 241–250. doi: 10.1080/04353676.1995.11880444.
- Arażny A., Przybylak R., Wyszynski P., Wawrzyniak T., Nawrot A. and Budzik T. 2018. Spatial variations in air temperature and humidity over Hornsund fjord (Spitsbergen) from 1 July 2014 to 30 June 2015. *Geografiska Annaler Series A, Physical Geography* 100: 27–43. doi: 10.1080/04353676.2017.1368832.
- Avila-Diaz A., Bromwich D.H., Wilson A.B., Justino F. and Wang S.H. 2021. Climate extremes across the North American Arctic in modern reanalyses. *Journal of Climate* 34: 2385–2410. doi: 10.1175/jcli-d-20-0093.1.
- Beel C.R., Lamoureux S.F. and Orwin J.F. 2018. Fluvial response to a period of hydrometeorological change and landscape disturbance in the Canadian High Arctic. *Geophysical Research Letters* 45: 10,446–10,455. doi: 10.1029/2018GL079660.

- Biskaborn B.K., Smith S.L., Noetzli J. *et al.* 2019. Permafrost is warming at a global scale. *Nature Communications* 10: 264. doi: 10.1038/s41467-018-08240-4.
- Błaszczyk M., Jania J.A. and Kolondra L. 2013. Fluctuations of tidewater glaciers in Hornsund Fjord (Southern Svalbard) since the beginning of the 20<sup>th</sup> century. *Polish Polar Research* 34: 327–352. doi: 10.2478/popore-2013-0024.
- Błaszczyk M., Ignatiuk D., Uszczyk A., Cielecka-Nowak K., Grabiec M., Jania J. A., Moskalik M. and Walczowski W. 2019. Freshwater input to the Arctic fjord Hornsund (Svalbard). *Polar Research* 38. doi: 10.33265/polar.v38.3506.
- Bokhorst S., Pedersen S.H., Brucker L. *et al.* 2016. Changing Arctic snow cover: a review of recent developments and assessment of future needs for observations, modelling, and impacts. *Ambio* 45: 516–537. doi: 10.1007/s13280-016-0770-0.
- Braithwaite R.J. 1995. Positive degree-day factors for ablation on the Greenland ice sheet studied by energy-balance modeling. *Journal of Glaciology* 41: 153–160.
- Christiansen H.H., Humlum O. and Eckerstorfer M. 2013. Central Svalbard 2000–2011 meteorological dynamics and periglacial landscape response. *Arctic, Antarctic, and Alpine Research* 45: 6–18. doi: 10.1657/1938-4246-45.1.6.
- Déry S.J., Hernández-Henríquez M.A., Burford J.E. and Wood E.F. 2009. Observational evidence of an intensifying hydrological cycle in northern Canada. *Geophysical Research Letters* 36: L13402. doi: 10.1029/2009gl038852.
- Diaconescu E.P., Mailhot A., Brown R. and Chaumont D. 2018. Evaluation of CORDEX-Arctic daily precipitation and temperature-based climate indices over Canadian Arctic land areas. *Climate Dynamics* 50: 2061–2085. doi: 10.1007/s00382-017-3736-4.
- European Climate Assessment & Dataset (ECA&D). 2013. Algorithm Theoretical Basis Document (ATBD), <https://www.ecad.eu/publications/index.php>, retrieved on 26.03.2019
- Etzelmüller B., Schuler T.V., Isaksen K., Christiansen H.H., Farbrot H. and Benestad R.E. 2011. Modelling the temperature evolution of Svalbard permafrost during the 20<sup>th</sup> and 21<sup>st</sup> century. *The Cryosphere* 5: 67–79. doi: 10.5194/tc-5-67-2011.
- Favaro E.A. and Lamoureux S.F. 2014. Antecedent controls on rainfall runoff response and sediment transport in a High Arctic Catchment. *Geografiska Annaler: Series A, Physical Geography* 96: 433–446. doi: 10.1111/geoa.12063.
- Førland E.J. and Hanssen-Bauer I. 2000. Increased precipitation in the Norwegian Arctic: True or false? *Climatic Change* 46: 485–509. doi: 10.1023/A:1005613304674.
- Førland E., Hanssen-Bauer I., Jónsson T., Kern-Hansen C., Nordli P., Tveito O. and Laursen E. 2002. Twentieth-century variations in temperature and precipitation in the Nordic Arctic. *Polar Record* 38: 203–210. doi:10.1017/S0032247400017721.
- Førland E.J., Benestad R., Hanssen-Bauer I., Haugen J.E. and Skaugen T.E. 2011. Temperature and precipitation development at Svalbard 1900–2100. *Advances in Meteorology* 2011. doi: 10.1155/2011/893790.
- Førland E., Isaksen K., Lutz J., Hanssen-Bauer I., Schuler T., Dobler A., Gjelten H. and Vikhamar-Schuler D. 2020. Measured and modeled historical precipitation trends for Svalbard. *Journal of Hydrometeorology* 21: 1279–1296. doi: 10.1175/jhm-d-19-0252.1.
- Frauenfeld O.W., Zhang T. and McCreight J.L. 2007. Northern hemisphere freezing/thawing index variations over the twentieth century. *International Journal of Climatology* 27: 47–63. doi: 10.1002/joc.1372.
- Grabiec M., Budzik T. and Głowacki P. 2012. Modelling and hindcasting of the mass balance of Werenskioldbreen (Southern Svalbard). *Arctic, Antarctic, and Alpine Research* 44: 164–179. doi: 10.1657/1938 4246-44.2.164.
- Hamed K.H. and Rao R.R.1998. A modified Mann-Kendall trend test for autocorrelated data. *Journal of Hydrology* 204: 182–196. doi: 10.1016/S0022-1694(97)00125-X.
- Hansen B.B., Isaksen K., Benestad R.E., Kohler J., Pedersen Å.Ø., Loe L.E., Coulson S.J., Larsen J.O. and Varpe Ø. 2014. Warmer and wetter winters: characteristics and implications of an

- extreme weather event in the High Arctic. *Environmental Research Letters* 9: 114021. doi: 10.1088/1748-9326/9/11/114021.
- Hanssen-Bauer I., Førland E.J., Hisdal H., Mayer S., Sandø A.B. and Sorteberg A. 2019. *Climate in Svalbard 2100 – a knowledge base for climate adaptation*. NCCS report no. 1/2019, Norwegian Environment Agency.
- Hinzman L.D., Deal C.J., McGuire A.D., Mernild S.H., Polyakov I.V. and Walsh J.E. 2013. Trajectory of the Arctic as an integrated system. *Ecological Applications* 23: 1837–1868. doi: 10.1890/11-1498.1.
- Hjort J., Ujanen J., Parviainen M., Tolgensbakk J. and Etzelmüller B. 2014. Transferability of geomorphological distribution models: Evaluation using solifluction features in subarctic and Arctic regions. *Geomorphology* 204: 165–176. doi: 10.1016/j.geomorph.2013.08.002.
- Hock R. 2003. Temperature Index Melt Modelling in mountain areas. *Journal of Hydrology* 282: 104–115. doi: 10.1016/S0022-1694(03)00257-9.
- Ignatiuk D.S., Błaszczyk M., Budzik T., Grabiec M., Jania J.A., Kondracka M., Laska M., Małarzewski Ł. and Stachnik Ł. 2022. A decade of glaciological and meteorological observations in the Arctic (Werenskioldbreen, Svalbard). *Earth System Science Data*. doi: 10.5194/essd-2021-464.
- IPCC 2019. Summary for Policymakers. In: Pörtner H.O., Roberts D.C., Masson-Delmotte V., Zhai P., Tignor M., Poloczanska E., Mintenbeck K., Alegria A., Nicolai M., Okem A., Petzold J., Rama B., Weyer N.M. (eds.) *IPCC Special Report on the Ocean and Cryosphere in a Changing Climate*. Cambridge University Press, Cambridge.
- IPCC 2021. Summary for Policymakers. In: Masson-Delmotte V. P., Zhai A., Pirani S. L., Connors C., Péan S., Berger N., Caud Y., Chen L., Goldfarb M. I., Gomis M., Huang K., Leitzell E., Lonnoy J.B.R., Matthews T. K., Maycock T., Waterfield O., Yelekçi R. Yu., Zhou B. (eds.) *Climate Change 2021: The Physical Science Basis. Contribution of Working Group I to the Sixth Assessment Report of the Intergovernmental Panel on Climate Change*. Cambridge University Press, Cambridge.
- Isaksen K., Benestad R.E., Harris C. and Sollid J.L. 2007a. Recent extreme near-surface permafrost temperatures on Svalbard in relation to future climate scenarios. *Geophysical Research Letters* 34: L17502. doi: 10.1029/2007GL031002.
- Isaksen K., Sollid J.L., Holmlund P. and Harris C. 2007b. Recent warming of mountain permafrost in Svalbard and Scandinavia. *Journal of Geophysical Research: Earth* 112: F02S04. doi: 10.1029/2006JF000522.
- Isaksen K., Nordli Ø., Førland E.J., Łupikasza E., Eastwood S. and Niedźwiedz T. 2016. Recent warming on Spitsbergen – Influence of atmospheric circulation and sea ice cover. *Journal of Geophysical Research: Atmospheres* 121: 11913–11931. doi: 10.1002/2016JD025606.
- Jahn A. 1976. Contemporaneous geomorphological processes in Longyeardalen, Vestspitsbergen (Svalbard). *Biuletyn Peryglacjalny* 26: 253–268.
- Kellerer-Pirklbauer A. 2018. Solifluction rates and environmental controls at local and regional scales in central Austria. *Norsk Geografisk Tidsskrift – Norwegian Journal of Geography* 72: 37–56. doi: 10.1080/00291951.2017.1399164.
- Landrum L. and Holland M.M. 2020. Extremes become routine in an emerging new Arctic. *Nature Climate Change* 10: 1108–1115. doi: <https://doi.org/10.1038/s41558-020-0892-z>.
- Larsson S. 1982. Geomorphological effects on the slopes of Longyear valley, Spitsbergen, after a heavy rainstorm in July 1972. *Geografiska Annaler* 64A: 105–125.
- Lewis T., Lafrenière M.J. and Lamoureaux S.F. 2012. Hydrochemical and sedimentary responses of paired High Arctic watersheds to unusual climate and permafrost disturbance, Cape Bounty, Melville Island, Canada. *Hydrological Processes* 26: 2003–2018. doi: 10.1002/hyp.8335.
- Lewis T. and Lamoureaux S.F. 2010. Twenty-first century discharge and sediment yield predictions in a small high Arctic watershed. *Global and Planetary Change* 71: 27–41. doi: 10.1016/j.



- gloplacha.2009.12.006.
- Lewandowski M., Polkowska Ż. and Ziaja W. (eds.) 2020. *Polish Polar Research: Green-and-White Paper*. Institute of Geophysics, Polish Academy of Sciences, Warsaw. doi: 10.25171/InstGeoph\_PAS\_Publs-2020-006, eISSN-2299-8020.
- Liu J., Wu D., Xu X., Ji M., Chen Q. and Wang X 2021. Projection of extreme precipitation induced by Arctic amplification over the Northern Hemisphere. *Environmental Research Letter* 16: 074012. doi: 10.1088/1748-9326/ac0acc.
- Łepkowska E. and Stachnik Ł. 2018. Which drivers control the suspended sediment flux in a High Arctic glacierized basin (Werenskioldbreen, Spitsbergen)? *Water* 10: 1408. doi: 10.3390/w10101408.
- Łupikasza E.B. and Cielecka-Nowak K. 2020. Changing probabilities of days with snow and rain in the Atlantic sector of the Arctic under the current warming trend. *Journal of Climate* 33: 2509–2532. doi: 10.1175/JCLI-D-19-0384.1.
- Łupikasza E. and Niedźwiedz T. 2019. The influence of mesoscale atmospheric circulation on Spitsbergen air temperature in periods of Arctic warming and cooling. *Journal of Geophysical Research – Atmospheres* 124: 5233–5250. doi: 10.1029/2018JD029443.
- Łupikasza E.B., Ignatiuk D., Grabiec M., Cielecka-Nowak K., Laska M., Jania J., Luks B., Uszczyk A. and Budzik T. 2019. The role of winter rain in the glacial system on Svalbard. *Water* 11: 2. doi: 10.3390/w11020334.
- Łupikasza E.B., Niedźwiedz T., Przybylak R. and Nordli Ø. 2021. Importance of regional indices of atmospheric circulation for periods of warming and cooling in Svalbard during 1920–2018. *International Journal of Climatology* 41: 3481–3502. doi: 10.1002/joc.7031.
- Majchrowska E., Ignatiuk D., Jania J., Marszałek H. and Wasik M. 2015. Seasonal and interannual variability in runoff from the Werenskioldbreen catchment, Spitsbergen. *Polish Polar Research* 36: 197–224. doi: 10.1515/popore-2015-0014.
- Marsz A.A. and Styszynska A. (eds.) 2013: *Climate and climate change at Hornsund, Svalbard*. The Publishing House of Gdynia Maritime University, Gdynia.
- Migała K., Pereyma J., Birkenmayer K., Ignatiuk D., Kabała C., Kasprzak M., Korabiewski B., Marszałek H., Matuła J., Migoń P., Rysiukiewicz M., Sikora S., Staško S., Wąsik M., Witkowski A. and Wojtuń B. 2013. Geographical environment in the vicinity of the Stanislaw Baranowski Polar Station – Werenskioldbreen. In: Zwoliński Z., Kostrzewski A., Pulina M. (eds.) *Ancient and modern geoecosystems of Spitsbergen*. Bogucki Wydawnictwo Naukowe, Poznań: 101–144.
- Muckenhuber S., Nilsen F., Korosov A. and Sandven S. 2016. Sea ice cover in Isfjorden and Hornsund, Svalbard (2000–2014) from remote sensing data. *The Cryosphere* 10: 149–158. doi: 10.5194/tc-10-149-2016.
- National Academies of Sciences, Engineering, and Medicine 2019. *Understanding Northern Latitude Vegetation Greening and Browning: Proceedings of a Workshop*. Washington, DC: The National Academies Press. doi: 10.17226/25423.
- Niedźwiedz T. 2013a. The atmospheric circulation. In: Marsz A.A. and Styszyńska A. (eds.) *Climate and climate change at Hornsund, Svalbard*. The Publishing House of Gdynia Maritime University, Gdynia: 57–74.
- Niedźwiedz T. 2013b. Influence of atmospheric circulation on the air temperature at Hornsund. In: Marsz, A.A. and Styszynska A. (eds.) *Climate and climate change at Hornsund, Svalbard*. The publishing house of Gdynia Maritime University, Gdynia: 165–172.
- Niedźwiedz T. 2020. *Kalendarz typów cyrkulacji atmosfery dla Spitsbergenu - zbiór komputerowy*, Uniwersytet Śląski, Katedra Klimatologii, Sosnowiec, <http://www.kk.wnoz.us.edu.pl/nauka/kalendarz-typow-cyrkulacji/>, accessed on 03.05.2021.
- NOAA 2020. National Centers for Environmental Information, Climate at a Glance, Global Time Series, available at: <https://www.ncdc.noaa.gov/cag/>, last access on 27.02.2020.
- Noël B., Jakobs C.L., van Pelt W.J.J., Lhermitte S., Wouters B., Kohler J., Hagen J.O., Luks B., Reijmer C.H., van de Berg W.J. and van den Broeke M.R. 2020. Low elevation of Svalbard

- glaciers drives high mass loss variability. *Nature Communications* 11: 4597. doi: 10.1038/s41467-020-18356-1.
- Nordli Ø., Wyszynski P., Gjeltén H., Isaksen K., Łupikasza E., Niedźwiedz T. and Przybylak R. 2020. Revisiting the extended Svalbard Airport monthly temperature series, and the compiled corresponding daily series 1898–2018. *Polar Research* 39: 3614. doi: 10.33265/polar.v39.3614.
- Norwegian Polar Institute. 2014. Kartdata Svalbard 1:100 000 (S100 Kartdata) / Map Data. Norwegian Polar Institute. doi: 10.21334/npolar.2014.645336c7.
- Nowak A. and Hodson A. 2013. Hydrological response of a High Arctic catchment to changing climate over the past 35 years: a case study of Bayelva watershed, Svalbard. *Polar Research* 32: 19691. doi: 10.3402/polar.v32i0.19691.
- Nowak A., Hodgkins R., Nikulina A., Osuch M., Wawrzyniak T., Kavan J., Lepakowska E., Majerska M., Romashova K., Vasilevich I., Sobota I. and Rachlewicz G. 2021. From land to fjords: The review of Svalbard hydrology from 1970 to 2019 (SvalHydro). In: Moreno-Ibáñez *et al.* (eds.) *SESS report 2020, Svalbard Integrated Arctic Earth Observing System*. Longyearbyen: 176–201. doi: 10.5281/zenodo.4294063.
- Opala-Owczarek M., Pirożnikow E., Owczarek P., Szymański W., Luks B., Kępski D., Szymanowski M., Wojtuń B. and Migala K. 2018. The influence of abiotic factors on the growth of two vascular plant species (*Saxifraga oppositifolia* and *Salix polaris*) in the High Arctic. *Catena* 163: 219–232. doi: 10.1016/j.catena.2017.12.018.
- Owczarek P., Latocha A., Wistuba M. and Malik I. 2013. Reconstruction of modern debris flow activity in the arctic environment with the use of dwarf shrubs (south-western Spitsbergen) - a new dendrochronological approach. *Zeitschrift für Geomorphologie* 57 Suppl. 3: 75–95. doi: 10.1127/0372-8854/2013/S-00145.
- Owczarek P., Nawrot A., Migala K., Malik I. and Korabiewski B. 2014. Flood-plain responses to contemporary climate change in small High-Arctic basins (Svalbard, Norway). *Boreas* 43: 384–402. doi: 10.1111/bor.12061.
- Owczarek P., Opala-Owczarek M. and Migala K. 2021. Post-1980s shift in the sensitivity of tundra vegetation to climate revealed by the first dendrochronological record from Bear Island (Bjørnøya), western Barents Sea. *Environmental Research Letter* 16: 014031. 10.1088/1748-9326/abd063.
- Panchen Z.A. and Gorelick R. 2017. Prediction of Arctic plant phenological sensitivity to climate change from historical records. *Ecology and Evolution* 7: 1325–1338. doi:10.1002/ece3.2702.
- Phoenix G.K. and Bjerke J. 2016. W. Arctic browning: extreme events and trends reversing arctic greening. *Global Change Biology* 22: 2960–2962. doi: 10.1111/gcb.13261.
- Pithan F. and Mauritsen T. 2014. Arctic amplification dominated by temperature feedbacks in contemporary climate models. *Nature Geoscience* 7: 181–184. doi: 10.1038/NNGEO2071.
- Przybylak R. 2002. Changes in seasonal and annual high-frequency air temperature variability in the Arctic from 1951 to 1990. *International Journal of Climatology* 22: 1017–1032. doi: 10.1002/joc.793.
- Przybylak R. 2016. *The Climate of the Arctic*. Second edition. Atmospheric and Oceanographic Sciences Library Vol. 52. Springer International Publishing Switzerland. doi: <https://doi.org/10.1007/978-3-319-21696-6>.
- Przybylak R. and Wyszynski P. 2020. Air temperature changes in the Arctic in the period 1951–2015 in the light of observational and reanalysis data. *Theoretical and Applied Climatology* 139: 75–94. doi: 10.1007/s00704-019-02952-3.
- Rapp A. and Nyberg R. 1988 Mass movements, nivation processes and climatic fluctuations in northern Scandinavian mountains. *Norwegian Journal of Geography* 42: 245–253. doi: 10.1080/00291958808552207.
- Rawlins M.A., Steele M., Holland M.M. *et al.* 2010. Analysis of the Arctic system for freshwater cycle intensification: Observations and expectations. *Journal of Climate* 23: 5715–5737. doi:

- 10.1175/2010jcli3421.1.
- Reichle L.M., Epstein H.E., Bhatt U.S., Raynolds M.K. and Walker D.A. 2018. Spatial heterogeneity of the temporal dynamics of arctic tundra vegetation. *Geophysical Research Letters* 45: 9206–9215. doi: 10.1029/2018GL078820.
- Rennett K.J., Roe G., Putkonen J. and Bitz C.M. 2009. Soil thermal and ecological impacts of rain on snow events in the circumpolar Arctic. *Journal of Climate* 22: 2302–2315. doi: 10.1175/2008JCLI2117.1.
- Schaefer K., Lantuit H., Romanovsky V., Schuur E. and Witt R. 2014. The impact of the permafrost carbon feedback on global climate. *Environmental Research Letters* 9: 085003. doi: 10.1088/1748-9326/9/8/085003.
- Schuler T.V., Kohler J., Elagina N., Hagen J.O.M., Hodson A.J., Jania J.A., Kääb A.M., Luks B., Malecki J., Moholdt G., Pohjola V.A., Sobota I. and Van Pelt W.J.J. 2020. Reconciling Svalbard glacier mass balance. *Frontiers in Earth Science* 8: 1–16. doi: 10.3389/feart.2020.00156.
- Serreze M.C., Crawford A.D. and Barrett A.P. 2015. Extreme daily precipitation events at Spitsbergen, an Arctic island. *International Journal of Climatology* 35: 4574–4588. doi: <https://doi.org/10.1002/joc.4308>.
- Shiklomanov A.I. and Lammers R.B. 2009. Record Russian river discharge in 2007 and the limits of analysis. *Environmental Research Letters* 4: 045015. doi: 10.1088/1748-9326/4/4/045015.
- Skagseth Ø., Furevik T., Ingvaldsen R., Loeng H., Mork K.A., Orvik K.A. and Ozhigin V. 2008. Volume and heat transports to the Arctic Ocean via the Norwegian and Barents Seas. In: Dickson B., Meincke J. and Rhines P. (eds.) *Arctic – subarctic ocean fluxes: defining the role of the northern seas in climate*. Springer, Dordrecht: 45–64. doi: 10.1007/978-1-4020-6774-7\_1.
- Smola Z., Tatarek A., Wiktor J.M., Kubiszyn A. and Węśławski J.M. 2017. Primary producers and production in Hornsund and Kongsfjorden – comparison of two fjord systems. *Polish Polar Research* 38: 351–373. doi: 10.1515/popore-2017-0013.
- Strand S.M., Christiansen H.H., Johansson M., Åkerman J. and Humlum O. 2021. Active layer thickening and controls on interannual variability in the Nordic Arctic compared to the circum-Arctic. *Permafrost and Periglacial Research* 32: 47–58. doi: 10.1002/ppp.2088.
- Stuefer S.L., Arp C.D., Kane D.L. and Liljedahl, A.K. 2017. Recent extreme runoff observations from coastal Arctic watersheds in Alaska. *Water Resources Research* 53 11: 9145–9163. doi: 10.1002/2017wr020567.
- Strzelecki M.C., Kasprzak M., Lim M., Swirad Z.M., Jaskólski M., Pawłowski Ł. and Modzel P. 2017. Cryo-conditioned rocky coast systems: A case study from Wilczekodden, Svalbard. *Science of The Total Environment* 607–608: 443–453. doi: 10.1016/j.scitotenv.2017.07.009.
- Vicente-Serrano S.M., Santiago Beguería S. and López-Moreno J.I. 2010. A multiscalar drought index sensitive to global warming: the standardized precipitation evapotranspiration index. *Journal of Climate* 23: 1696–1718. doi: 10.1175/2009JCLI2909.1.
- Walczowski W. and Piechura J. 2011. Influence of the west Spitsbergen current on the local climate. *International Journal of Climatology* 31: 1088–1093. doi: 10.1002/joc.2338.
- Walsh J.E., Ballinger T.J., Euskirchen E.S., Hanna E., Mård J., Overland J.E., Tangen H. and Vihma T. 2020. Extreme weather and climate events in northern areas: A review. *Earth-Science Reviews* 209: doi: 10.1016/j.earscirev.2020.103324.
- Warwick R.M., Emblow C., Feral J.P., Hummel H., Van Avesaath P. and Heip C. 2003. European marine biodiversity research sites. Report of the European Concerted Action: BIOMARE. NIOO-CEME, Yerseke, The Netherlands..
- Wawrzyniak T. and Osuch M. 2019. A consistent High Arctic climatological dataset (1979–2018) of the Polish Polar Station Hornsund (SW Spitsbergen, Svalbard). *Pangea*: doi: 10.1594/PANGAEA.909042.
- Wawrzyniak T. and Osuch M. 2020. A 40-year High Arctic climatological dataset of the Polish Polar Station Hornsund (SW Spitsbergen, Svalbard). *Earth System Science Data* 12: 805–815.

- doi: 10.5194/essd-12-805-2020.
- Weijers S., Wagner-Cr mer F., Sass-Klaassen U., Broekman R. and Rozema J. 2013. Reconstructing High Arctic growing season intensity from shoot length growth of a dwarf shrub. *The Holocene* 23: 721–731. doi: 10.1177/0959683612470178.
- Weydmann A. and Kwasniewski S. 2008. Distribution of *Calanus* populations in a glaciated fjord in the Arctic (Hornsund, Spitsbergen) – the interplay between biological and physical factors. *Polar Biology* 31: 1023–1035. doi: 10.1007/s00300-008-0441-0.
- Węslawski J.M., Urbański J., Głuchowska M., Grzelak K., Kotwicki L., Kwaśniewski S., Legeżyńska J., Wiktor J., Włodarska-Kowalczyk M., Zaborska A., Zaj czkowski M. and Stempniewicz L. 2017. Can seabirds modify carbon burial in fjords? *Oceanologia* 59: 603–611. doi: 10.1016/j.oceano.2017.01.006.
- Wickstrom S., Jonassen M.O., Cassano J.J. and Vihma T. 2020. Present temperature, precipitation, and rain-on-snow climate in Svalbard. *Journal of Geophysical Research-Atmospheres* 125: e2019JD032155. doi: 10.1029/2019JD032155.
- WMO 2012. Standardized Precipitation Index User Guide, WMO-No. 1090, [https://library.wmo.int/doc\\_num.php?explnum\\_id=7768](https://library.wmo.int/doc_num.php?explnum_id=7768), accessed on 03.10.2020,
- WMO&GWP 2016. Handbook of drought indicators and indices (M. Svoboda and B.A. Fuchs). Integrated Drought Management Programme (IDMP), Integrated Drought Management Tools and Guidelines Series 2. Geneva.
- Yang D., Shi X. and Marsh P. 2015. Variability and extreme of Mackenzie River daily discharge during 1973– 2011. *Quaternary International* 380–381: 159–168. doi: 10.1016/j.quaint.2014.09.023.
- Young K.L., Lafreni re M.J., Lamoureux S.F., Abnizova A. and Miller E.A. 2015. Recent multi-year streamflow regimes and water budgets of hillslope catchments in the Canadian High Arctic: evaluation and comparison to other small Arctic watershed studies. *Hydrology Research* 46: 533–550. doi: 10.2166/nh.2014.004.

Received 14 June 2022

Accepted 22 December 2022